Finite Volume Coastal Ocean Model (FVCOM) 3D Hydrodynamic Model Comparison

Haosheng Huang
Department of Oceanography and Coastal Sciences
School of the Coast and Environment
Louisiana State University, Baton Rouge, LA 70803

Prepared for the Texas Water Development Board (TWDB)
Austin Texas

Final Report

May 17, 2011

Finite Volume Coastal Ocean Model (FVCOM) 3D Hydrodynamic Model Comparison

Haosheng Huang
Department of Oceanography and Coastal Sciences
School of the Coast and Environment
Louisiana State University, Baton Rouge, LA 70803

Prepared for the Texas Water Development Board (TWDB)
Austin Texas

Final Report

May 17, 2011

Summary

The purpose of this Research and Planning Fund contract is for comparing the performance of various hydrodynamic models on a common benchmark problem. The Corpus Christi Bay benchmark problem is designed by TWDB staff and includes a dataset which is used for calibration of the model and a separate dataset which is for model verification. The application of the Finite-Volume Coastal Ocean Model (FVCOM) to this benchmark problem enables TWDB to evaluate the strengths and weaknesses of the model for use in predicting the three-dimensional circulation and salinity transport in bay and estuary systems on the Texas coast.

FVCOM experiments have been run to simulate the three-dimensional circulation of Corpus Christi Bay driven by buoyancy, tides, and winds. Comparisons between observations and model simulation show that FVCOM is very accurate in predicting the sea level oscillations. The average correlation coefficient and Index of Agreement are 0.96 and 0.97, respectively, for the total water level elevation, and 0.97 and 0.97, respectively, for the sub-tidal, wind-driven oscillations. The velocity simulation is visually consistent with available ADCP measurements. However, no quantitative assessment can be done due to the short duration and non-uniform interval of observed current time series. The salinity simulation is not as satisfactory as sea level and current simulations. Possible reasons for discrepancies are pointed out. Recommendations for model improvement are provided.

Finite Volume Coastal Ocean Model (FVCOM) 3D Hydrodynamic Model Comparison

1. Model description

The Finite-Volume Coastal Ocean Model (FVCOM) used in this study was jointly developed by University of Massachusetts – Dartmouth and Woods Hole Oceanographic Institution modeling research teams. It is a three-dimensional, unstructured-grid, free-surface, primitive equation ocean model (Chen et al., 2003; Chen et al., 2006). Unlike numerical models using finite-difference or finite-element method, FVCOM employs the finite-volume method that discretizes the integral form of governing equations and numerically solves them by flux calculation over a triangular mesh. Therefore, it is better in guaranteeing mass conservation in both the individual control element and the entire computational domain.

Besides the above mentioned features of finite-volume method and triangular grid, FVCOM is very similar, in all other aspects, to traditional ocean models, such as Princeton Ocean Model (POM). For example FVCOM uses a σ-coordinate in the vertical, incorporates the Mellor and Yamada (1982) level-2.5 turbulence closure sub-model as modified by Galperin et al. (1988) for flow-dependent vertical mixing coefficients, uses the Smagorinsky (1963) formulation for calculating horizontal mixing coefficients, and employs a logarithmic profile to simulate the bottom boundary layer and determine the bottom friction. In addition, FVCOM also uses a mode-splitting technique to solve the momentum equations with two distinct time steps for computational efficiency, i.e., external and internal mode time steps to accommodate the faster and slower barotropic and baroclinic responses, respectively.

Instead of a staggered C-grid (with horizontal velocity components on the sides and scalar variables in the center) used by POM, FVCOM uses a grid arrangement such that all scalar variables are solved at the grid nodes, whereas velocity is solved at the grid centers. The use of a σ-coordinate in the vertical allows for a free surface and irregular bottom topography mapped onto a regular domain.

For other FVCOM features and a detailed description of FVCOM discrete equations and various boundary conditions, please consult FVCOM manual (Chen et al., 2006).

2. Model configuration

The model domain and nonoverlapping unstructured triangular grids are shown in Figure 1. The domain encompasses the Aransas Bay, Nueces Bay, Corpus Christi Bay, Baffin Bay, and the upper Laguna Madre. The Gulf Intracoastal Waterway (GIWW) flows through the region. The northern and southern ends of GIWW in this computational domain are treated as closed boundaries due to lack of boundary conditions. By arching the open boundary in the Gulf of Mexico (GOM), the model domain also includes a portion of the inner shelf out to about 15 km from the barrier islands. The entire model

grid consists of 10877 nodes and 18862 triangular cells in the horizontal and 31 evenly distributed σ levels in the vertical. Horizontal resolution varies from 30 m in the ship channel and intracoastal waterway to about 600 m in the bays, gradually expanding to 1.8 km near the open boundary. Vertical resolution varies from 0.02 m to 1 m depending on water depth (Figure 2). Based on the CFL condition, computational time steps of 1 s and 10 s are used for the external and internal modes, respectively. For the present study the model is initialized on January 1, 2000 and run to December 31, 2000. The period January 1 to January 10, 2000 is the model ramp-up time during which all model forcings increase from zero to their full strengths following a hyperbolic tangent function. The model analysis interval is from January 10, 2000 to the end of the year 2000.

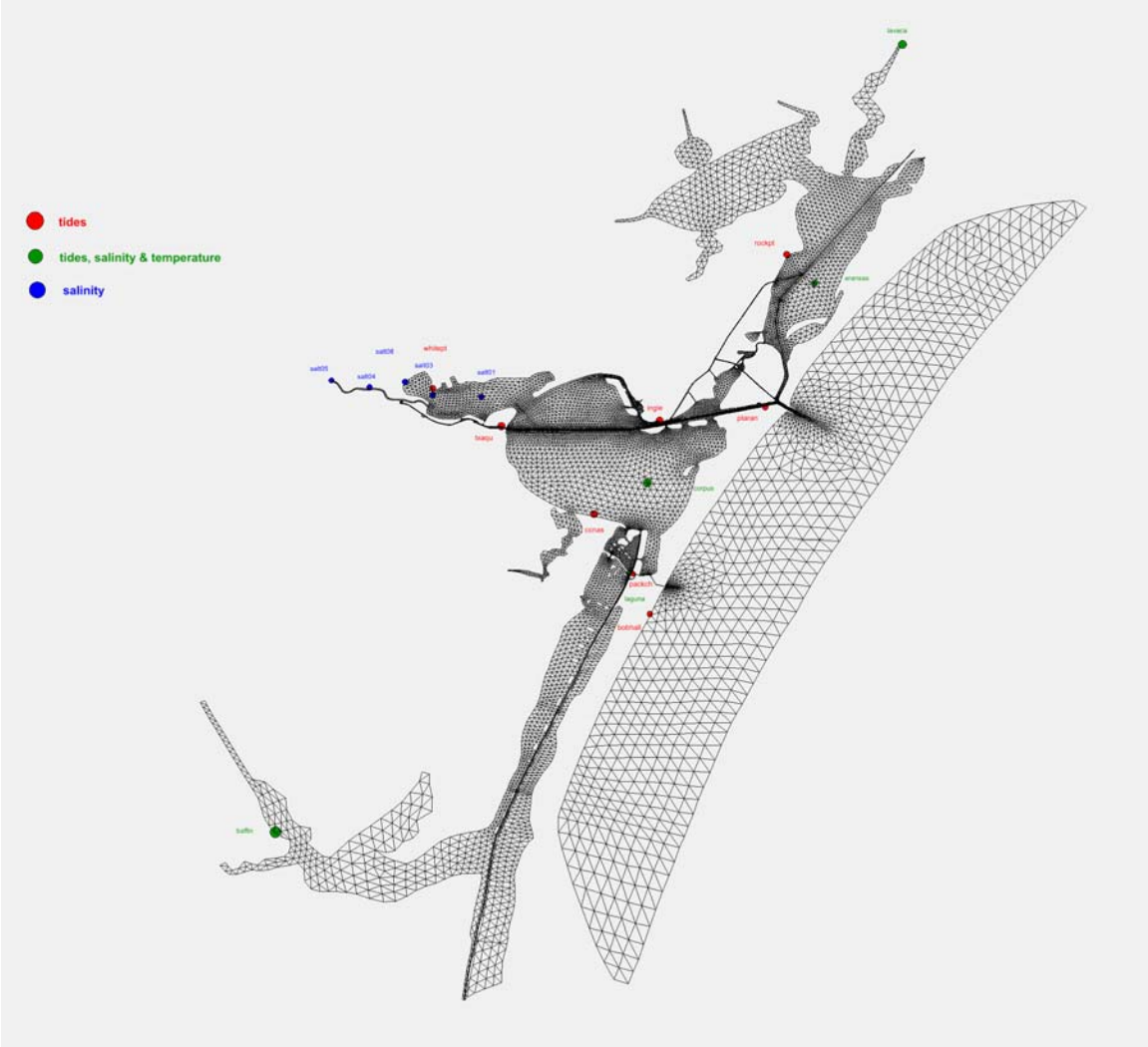

Fig. 1 Corpus Christi Bay FVCOM numerical grid and station locations used for water elevation, velocity and salinity comparison.

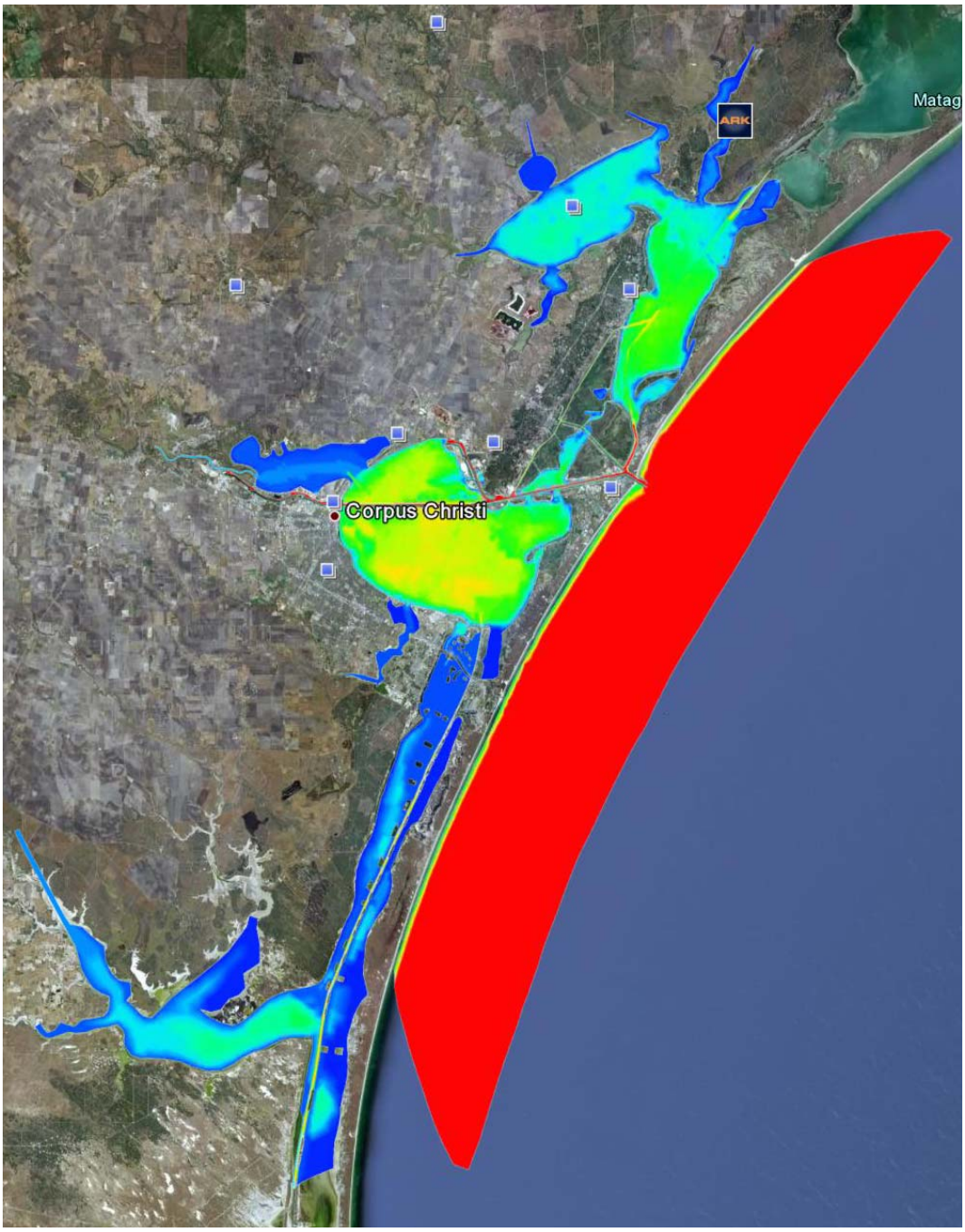

Fig. 2 Corpus Christi Bay FVCOM numerical model bathymetry

3. Model forcing functions and initial conditions

3.1 Elevation boundary condition

Along with steric effects, coastal sea level fluctuations are in response to tides [η_T (x, t)] and weather (by wind and atmosphere pressure) [η_M (t)]. How to specify these at the open boundary, so that the model can calculate correct values over the computational

interior, is a critical issue. In this study we use observed elevation data at Bob Hall Pier (Figure 1) and assume it can be applied uniformly to all open boundary nodes. The uniformity assumption may cause errors if tidal harmonics and wind-driven sea level oscillation have large spatial variation near the inner shelf in the study area. Fortunately, numerical calculation results shown in the next section indicate that this is not the case.

The sampling interval of water level time series at Bob Hall Pier is 6 minutes. It is relative to the mean sea level (MSL). There are very few gaps in the time series that are filled using linear interpolation method. Figure 3 shows the water level time series.

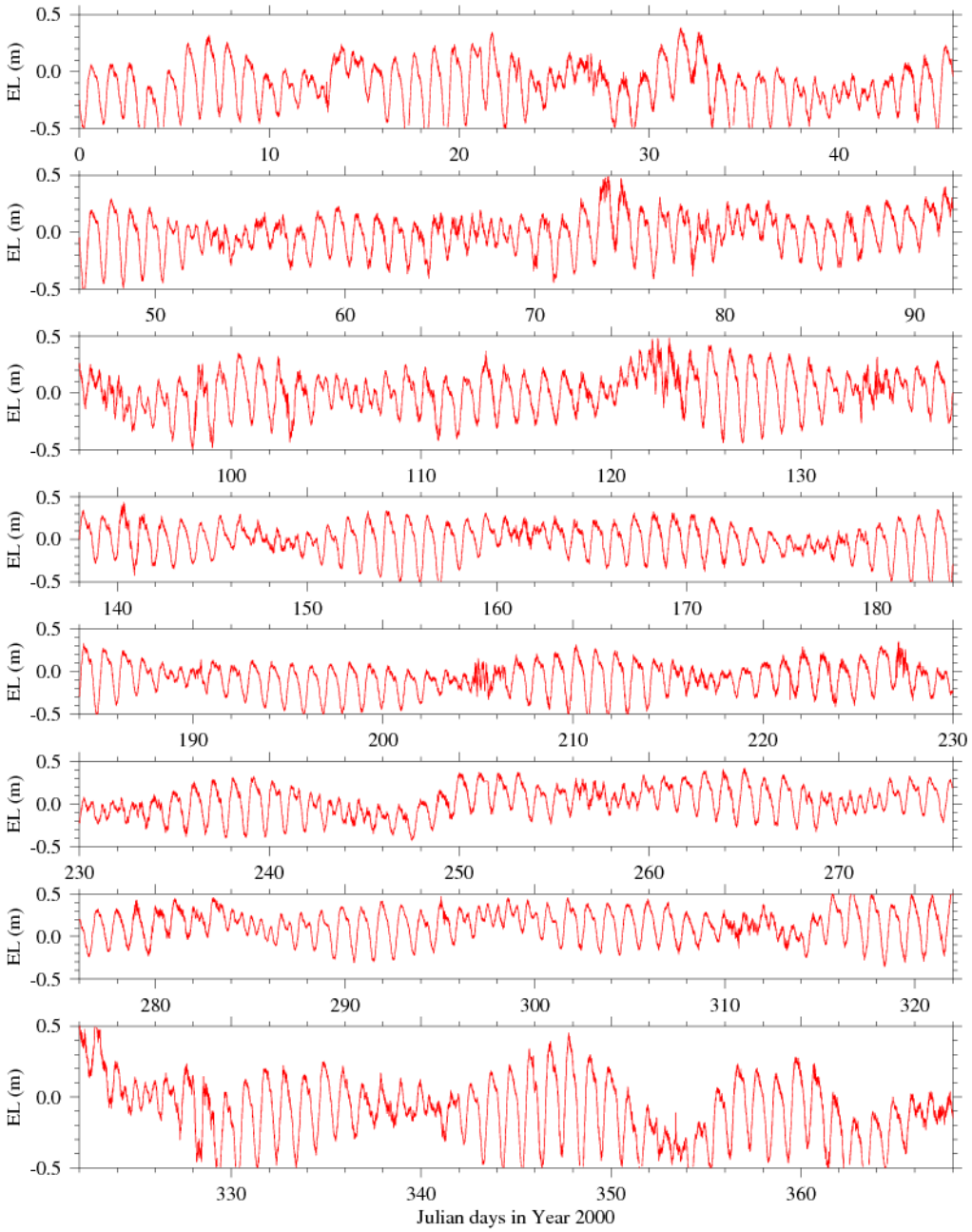

Figure 3. Water level time series for station Bob Hall Pier for Year 2000.

3.2 Salinity boundary condition

Typical of coastal studies we hold temperature constant at 20 ºC, based on the assumption that the baroclinic forcing in the Corpus Christi Bay and adjacent inner shelf is mainly determined by the salinity gradient rather than by the temperature gradient variations. When the salt flux is directed out of the computational domain along the open boundary, the salinity is calculated from the salt advection equation by applying a second-order upwind scheme, whereas when the salt flux is directed into the computational domain, the salinity is relaxed towards observed values (relaxation time scale is 20 days, salinity data from biweekly samples taken offshore by the Texas Parks and Wildlife Department) that is shown in Figure 4. The abrupt salinity changes in Figure 4 indicate that there may exist some coastal processes whose dynamics are not well resolved by our limited domain model, or the observed salinity time series may have some errors.

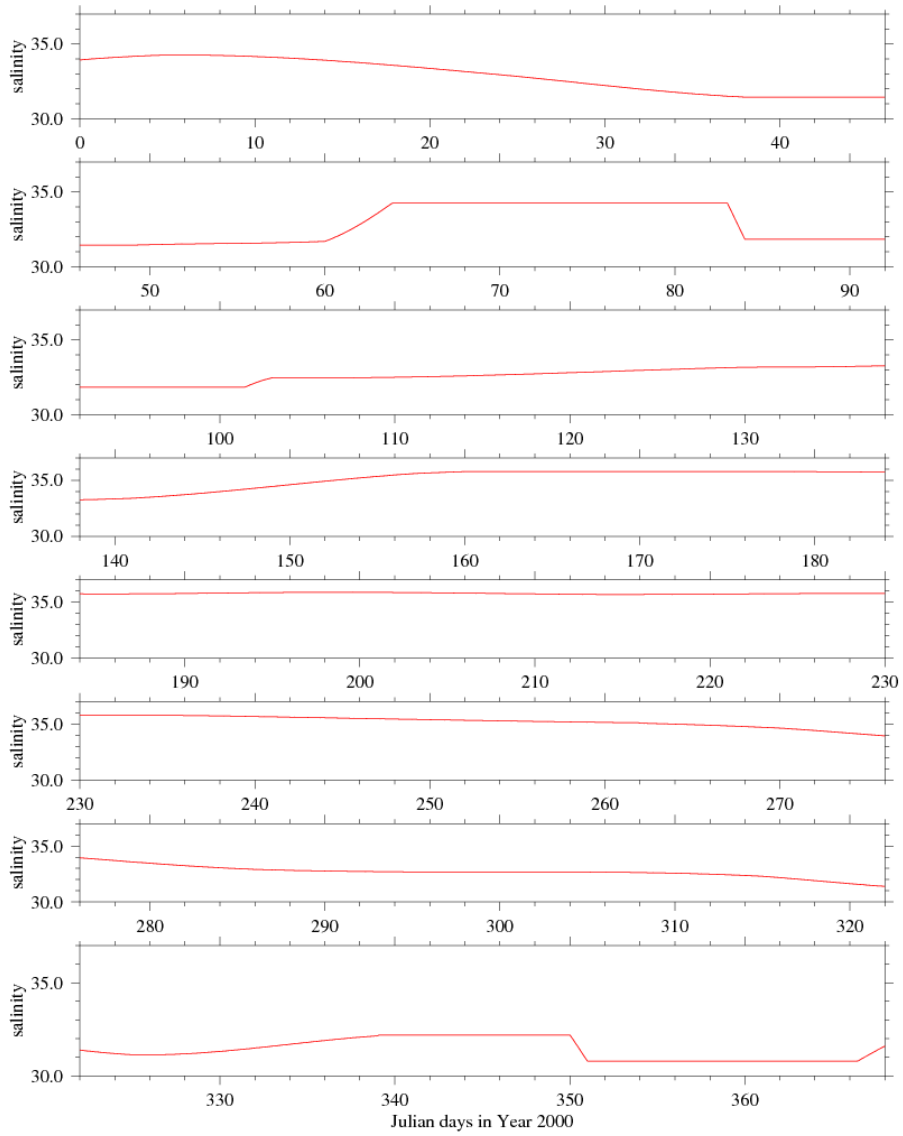

Figure 4. Salinity time series at offshore stations for Year 2000, which is used for open boundary salinity relaxation.

3.3 River inflows

South Texas bays are characterized by broad climate variations that alternate between wet and dry cycles (Montagna and Kalke, 1995). There are seven relatively large fresh water inflows inside the computation domain. They are from the Cavasso, Copano, Mission, Aransas, Nueces, Oso, and Baffin rivers (Figure 1). Other small creeks and streams are not considered in this calculation. To accommodate these sources fresh water (salinity specified as zero) is distributed amongst 14 grid nodes and injected into the computational domain as a volume flux boundary condition using the method of Chen et al. (2006). Daily discharge data at these node positions for the year 2000 period are calculated from a hydrological model developed by Texas Water Development Board (TWDB), which combines USGS gage flow data with coastal rainfall runoff estimates and reported diversions and return flows below the gage (http://midgewater.twdb.state.tx.us/bays_estuaries/hydrologypage.html). Time series for individual inflows are shown in Figure 5. The annually averaged freshwater fluxes for Year 2000 are 5.8 $m^3 s^{-1}$, 0.2 $m^3 s^{-1}$, 2.1 $m^3 s^{-1}$, 3.9 $m^3 s^{-1}$, 6.4 $m^3 s^{-1}$, 1.2 $m^3 s^{-1}$, and 4.1 $m^3 s^{-1}$, respectively, for the Cavasso, Copano, Mission, Aransas, Nueces, Oso, and Baffin rivers. Hence, the year 2000 can be classified as a dry year. As can be seen in Figure 5, most of the freshwaters are concentrated in several peak inflow events that occurred mainly in spring (March, May, and June) and fall (October and November) seasons. Other times the freshwater inflows are close to zero except for the Nueces River.

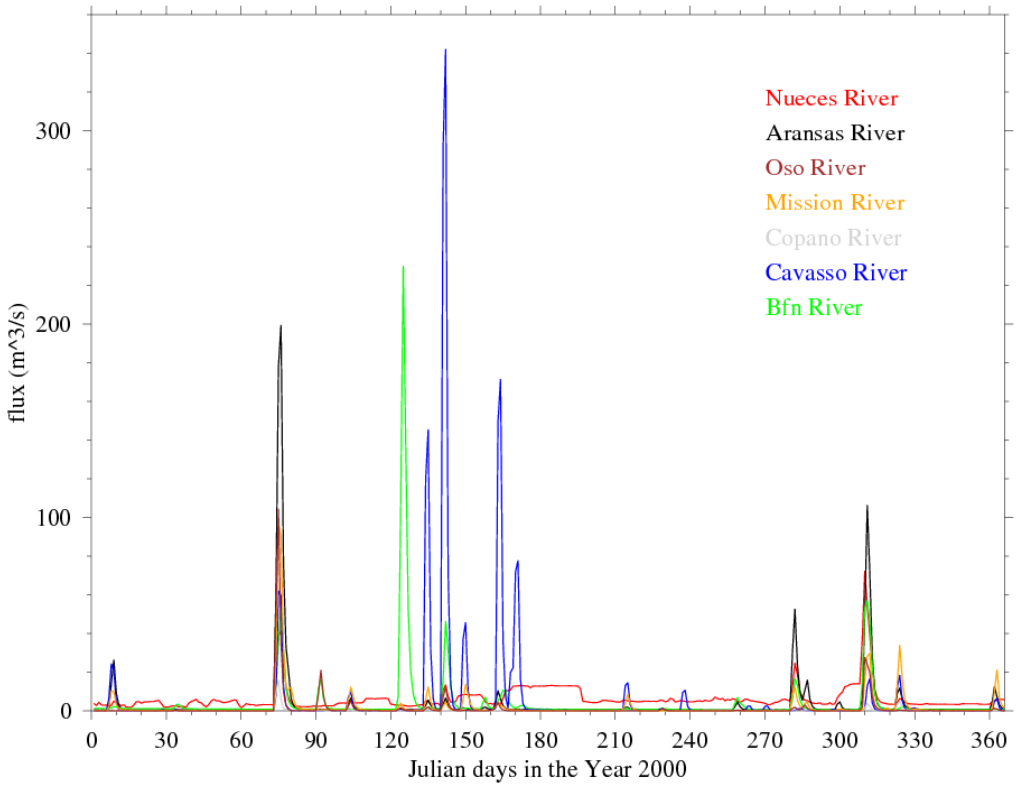

Figure 5. Daily values of the freshwater inflows from the seven rivers in computation domain for Year 2000.

There are two power plants in the area that take in cooling waters from the bay and discharge them at other locations. The boundary conditions for these intake and discharge ports are very similar to the river discharge nodes for momentum and mass conservation equations. The salinity boundary condition needs special treatment. For discharge point, its salinity is set to be equal to the salinity of corresponding intake node. The salinity at intake node is calculated using an upwind scheme for salinity advection term. Since at intake site the velocity always points from bay to the power plant, this guarantees that the boundary treatment is physically sound and numerical stable. In current FVCOM version no power plant intake and discharge sites are considered. New subroutines are written to implement the above mentioned boundary treatment. The code is written in Fortran90 with MPI. The time series of volume flux of the two power plants are relatively uniform, with annually averaged transport of 16.8 m^3 s^{-1} (Nueces Bay Power Plant) and 19.2 m^3 s^{-1} (Barney Davis Power Plant) respectively (figure not shown).

3.4 Meteorological forcing functions

Spatially uniform wind stress is used over the computational domain. Hourly wind speed and direction data collected at Texas Coastal Ocean Observation Network (TCOON) Ingleside station are applied from January 1 to December 31, 2000, with a few short wind data gaps filled using a linear interpolation algorithm. The wind vector time series (subsample every 6 hours) is shown in Figure 6. Southeastly wind prevails in the series, especially from April to August (from day 80 to day 250). The annual mean wind speed is 4.3 m s^{-1}. Wind stress is calculated according to the bulk formula of Large and Pond (1981).

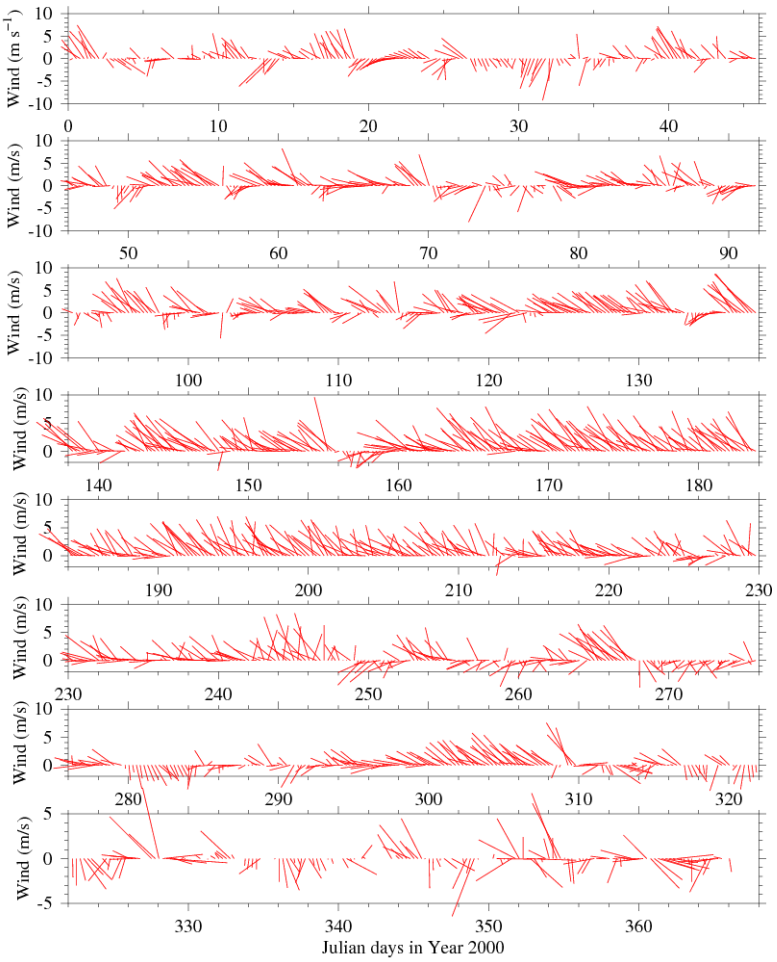

Figure 6. Time series of hourly wind vector (sub-sampled every 6 hours) used in the FVCOM model

No air pressure data are available, which should be used to

adjust the observed sea level for comparison with the model simulated sea level since for this study air pressure is held constant in numerical calculation. This may account for some of the discrepancies found between observed and modeled water elevation in the next section. Another alternative is to use meteorological products, such as from NOAA NCEP (National Centers for Environmental Prediction) regional reanalysis product (http://www.cdc.noaa.gov/cdc/data.narr.html). But I haven't done that.

Spatially uniform precipitation and evaporation rates are used over the computational domain. Daily data collected at the Naval Air Station in Corpus Christi Bay are applied from January 1 to December 31, 2000 (Figure 7). The annual mean precipitation and evaporation rates are 0.5593 m yr^{-1} and 1.3215 m yr^{-1}, respectively, for year 2000. Obviously, evaporation is much higher than precipitation in this area.

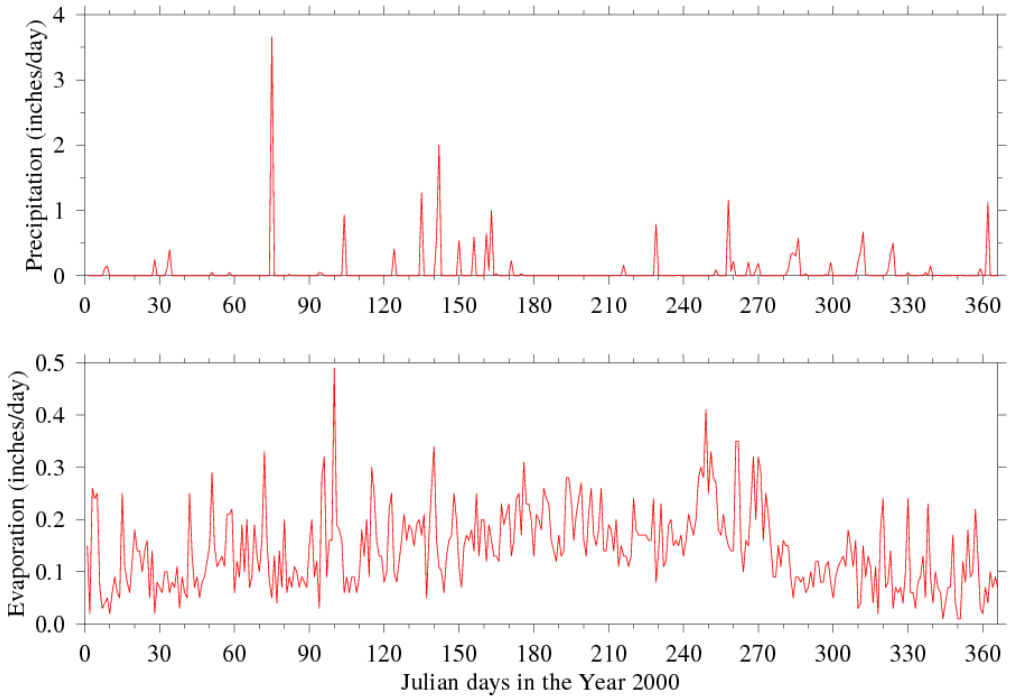

Figure 7. Daily values of precipitation and evaporation rate (inches/day) for Year 2000.

One issue which is related to salinity calculation needs further clarification. Current version of FVCOM uses upwind biased finite-volume method to calculate the horizontal advective and diffusive fluxes across the interface of control volumes. This doesn't cause any problem. However, in the vertical direction the fluxes are calculated using a finite-volume method which is equivalent to central in space finite-difference scheme. The central difference scheme inevitably causes the well-known Gibbs oscillations (a.k.a. overshooting and undershooting) in regions of unsolved gradients in the solution (LeVeque, 2002). So in a pure precipitation test case (assuming no velocity and no mixing, the only forcing to the model is a constant precipitation rate at sea surface in a square domain), the salinity at the surface is zero (we assume the rain is freshwater) and the thickness of this fresh surface layer increases linearly with time. Below surface

layer the salinity keeps the same as initial value (we assume the initial salinity is 30 ppt in the whole domain). A salinity jump will appear in the vertical as more and more rains pour at the surface. The vertical location of this interface (i.e. salinity jump) is equal to initial water depth ($z = H_{initial}$). In simulating this salinity jump, the central difference scheme causes overshooting and undershooting, so that salinity values smaller than 0 ppt and greater than 30 ppt appear in the simulation. Similar overshooting and undershooting appears in the pure evaporation experiment as well. To avoid the overshooting and undershooting problem, flux limiters are introduced in the vertical advective flux calculation (LeVeque, 2002). The flux limiters tested include minmod, superbee, MC (monotonized central-difference), and van Leer (LeVeque, 2002). We found that MC limiter gives the best result comparing to the analytic solution. Therefore, MC limiter is used in the Corpus Christi Bay 3-D baroclinic run.

In addition, surface salinity boundary condition is specified in a freshwater flux form following the formula in Huang (1993), which guarantees the conservation of salt in the computation domain. The surface precipitation/evaporation boundary condition used in many existing models is actually incorrect since it introduces a salt flux at the sea surface (for example, see POM manual and discussion in Huang (1993)).

3.5 Initial conditions

The initial values of elevation and velocity are specified as zero throughout the computational domain. By running a separate, two-dimensional finite-element hydrodynamics and salinity model for the same numerical grid that is routinely maintained at Texas Water Development Board (TWDB) we obtained the initial horizontal salinity distribution for this three-dimensional simulation. We took the two-dimensional model output at 00:00 AM January 1, 2000 (Figure 8) and assume that salinity is uniformly distributed in the vertical.

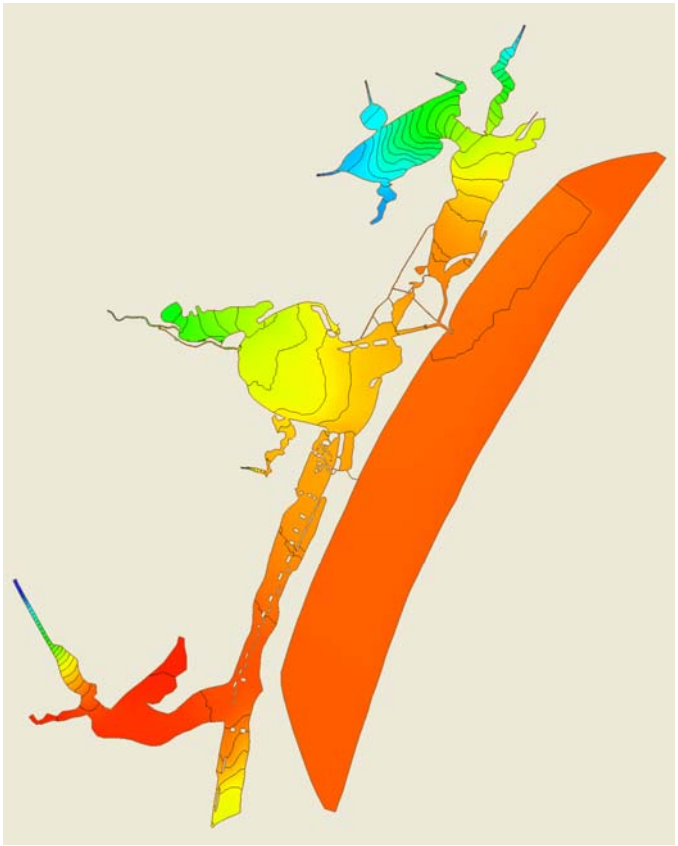

Figure 8. FVCOM initial salinity condition

4. Comparisons between model simulations and observations

The most abundant data set available for comparison with the model simulation is that of sea level. Velocity and salinity data are more limited. Three types of comparisons are shown to establish some degree of model veracity: hourly times series, low-pass filtered time series, and seasonal means. For sea level we use data from TCOON tide gauges at Corpus Christi Bay Naval Air Station, Packery Channel, Ingleside, Texas Aquarium, Port Aransas, White Point, and Rockport (Figure 1). The water level data provided by TWDB have not been referenced to mean sea level (MSL) and seem to have some outliers. So they are not used in the comparison. For velocity we have six acoustic Doppler current profiler (ADCP) records sampled within the deep shipping channel at various locations. However, the data are only available for three-day period (May 5 – May 7, 2000, see http://midgewater.twdb.state.tx.us/bays_estuaries/studies/cor00main.html). The station locations are shown in Figure 9. Salinity data are limited to CTD samples at three stations for the same period of time. Additional salinity observations are provided by Nueces River Authority and the Division of Nearshore Research for locales inside Nueces Bay, Texas Water Development Board (TWDB) and Corpus Christi Bay Hypoxia program (Paul Montagna, personal communication) for locales in Corpus Christi Bay.

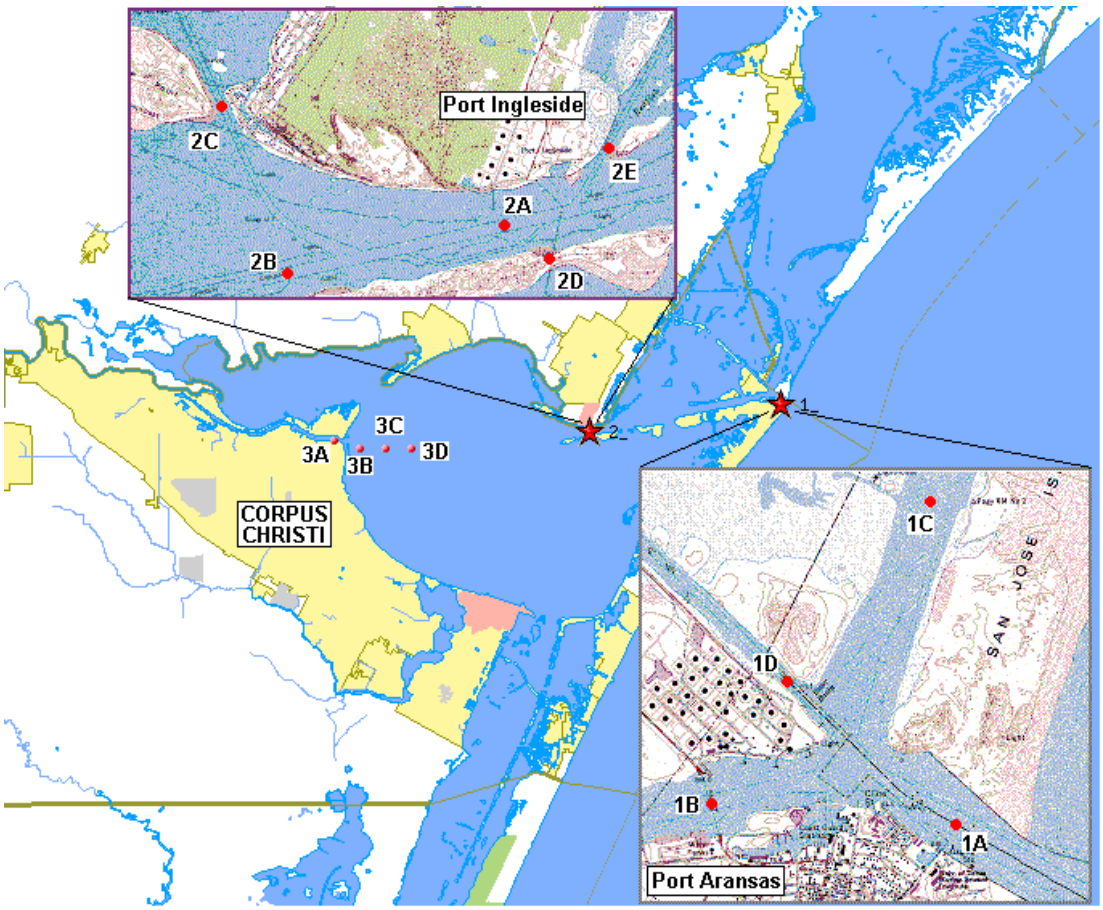

Figure 9. Station map of Corpus Christi Bay 2000 intensive inflow survey (May 5 – May 7, 2000) (taken from http://midgewater.twdb.state.tx.us/bays_estuaries/studies/cor00main.html)

4.1 Sea level

Comparisons of time series between observed (6-min sampling interval) and modeled (hourly sampling interval) sea levels are shown in Figures 10 - 16, along with the hourly wind velocity vectors used to force the model. Visually we see agreement in both amplitude and phase at all seven stations, and we note that the amplitude agreements are best when the winds are light. The model also reproduces the tropic-equatorial tide cycle. This demonstrates a degree of validity in the use of Bob Hall Pier water level record as elevation open boundary condition.

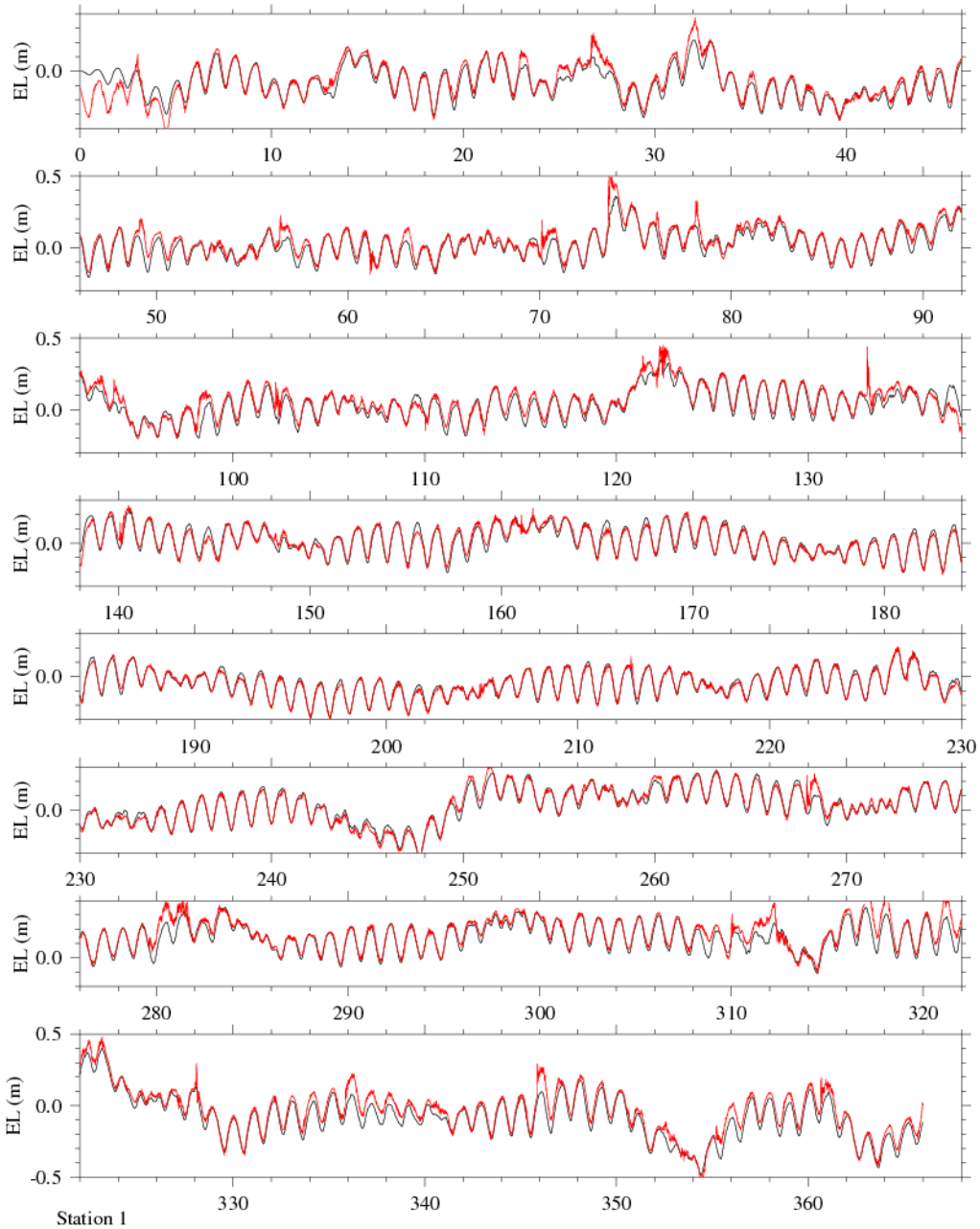

Figure 10. Time series comparison for sea levels observed (red) and modeled (black) at Corpus Christi Bay Naval Air Station.

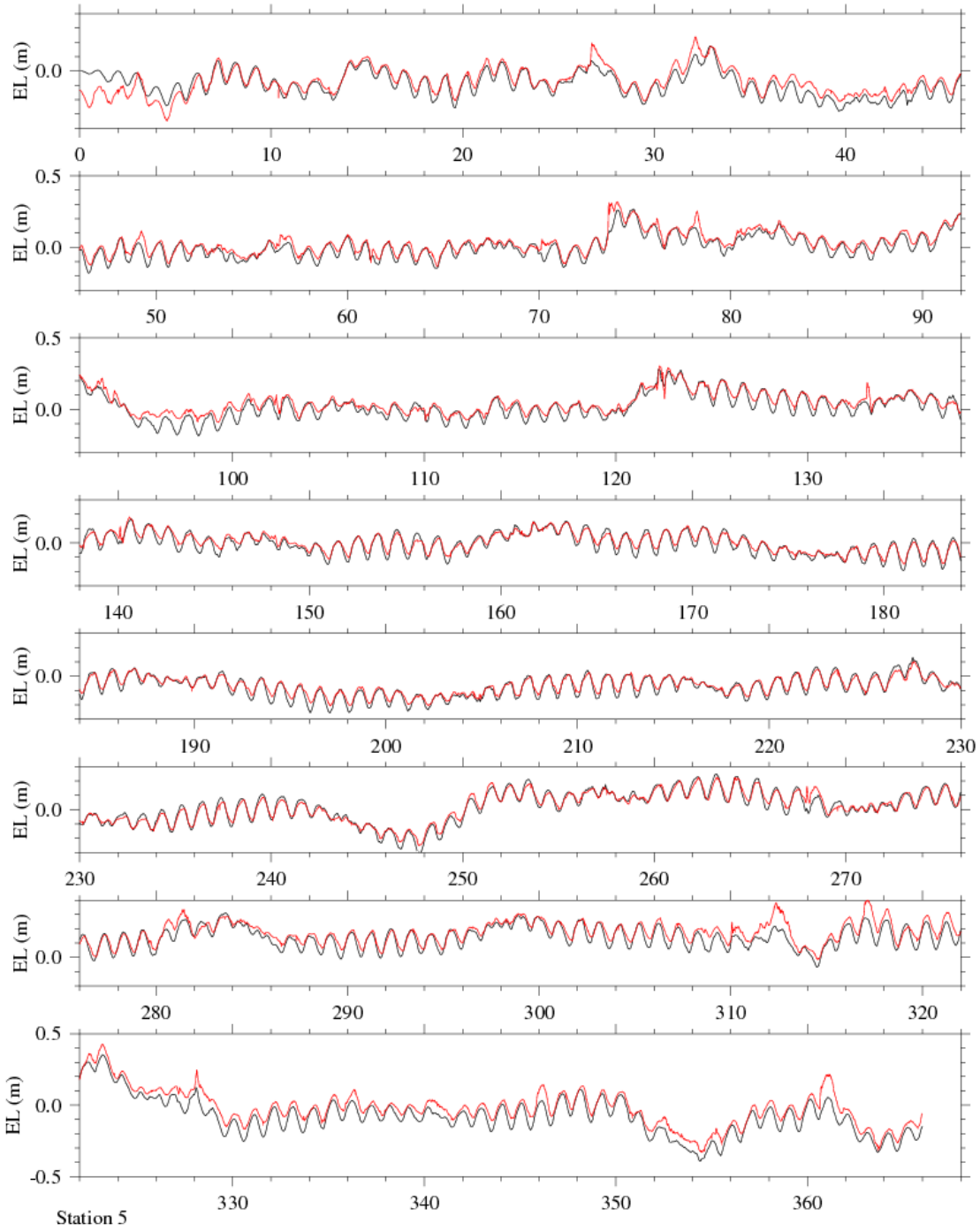

Figure 11. Time series comparison for sea levels observed (red) and modeled (black) at Packery Channel.

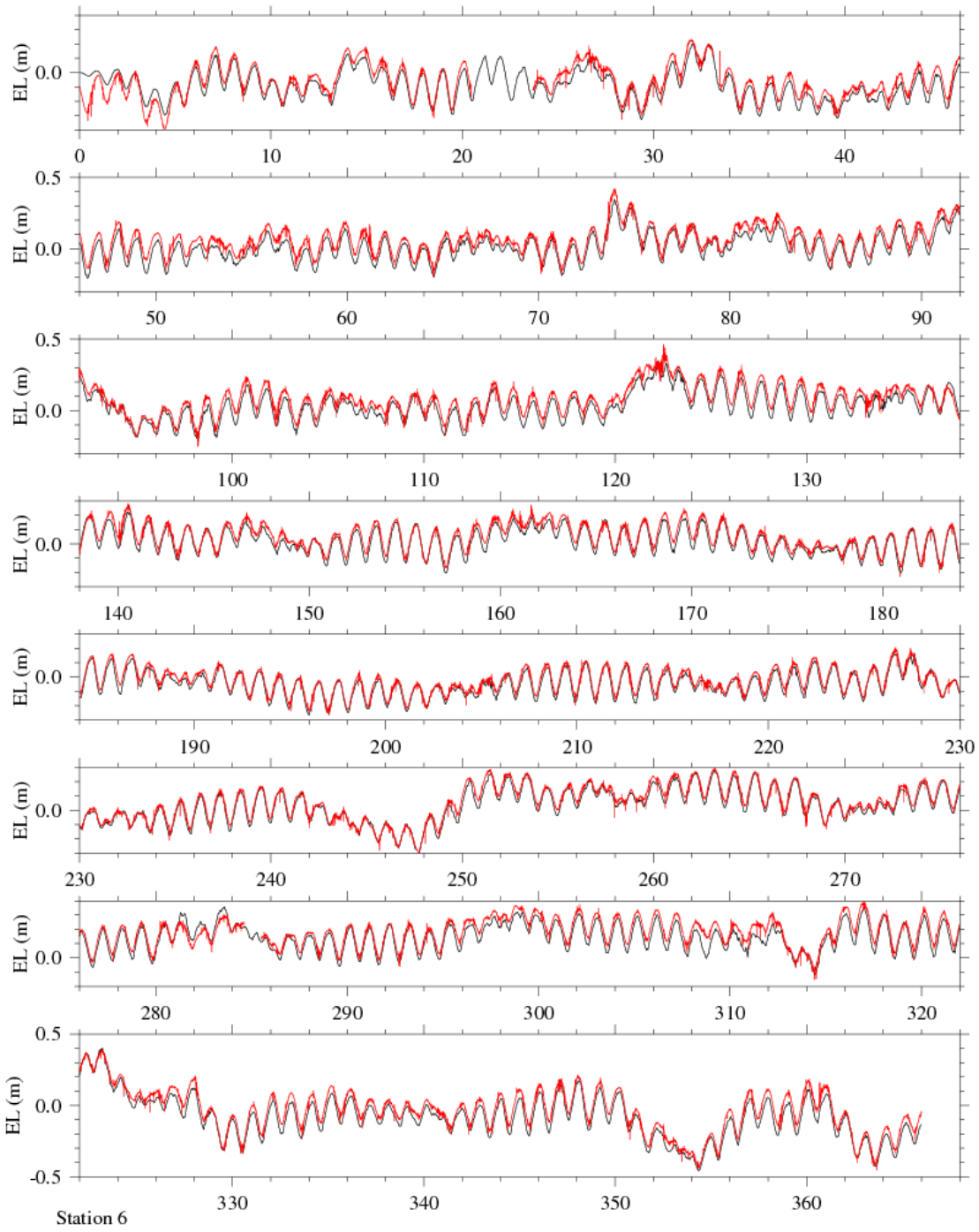

Figure 12. Time series comparison for sea levels observed (red) and modeled (black) at Ingleside.

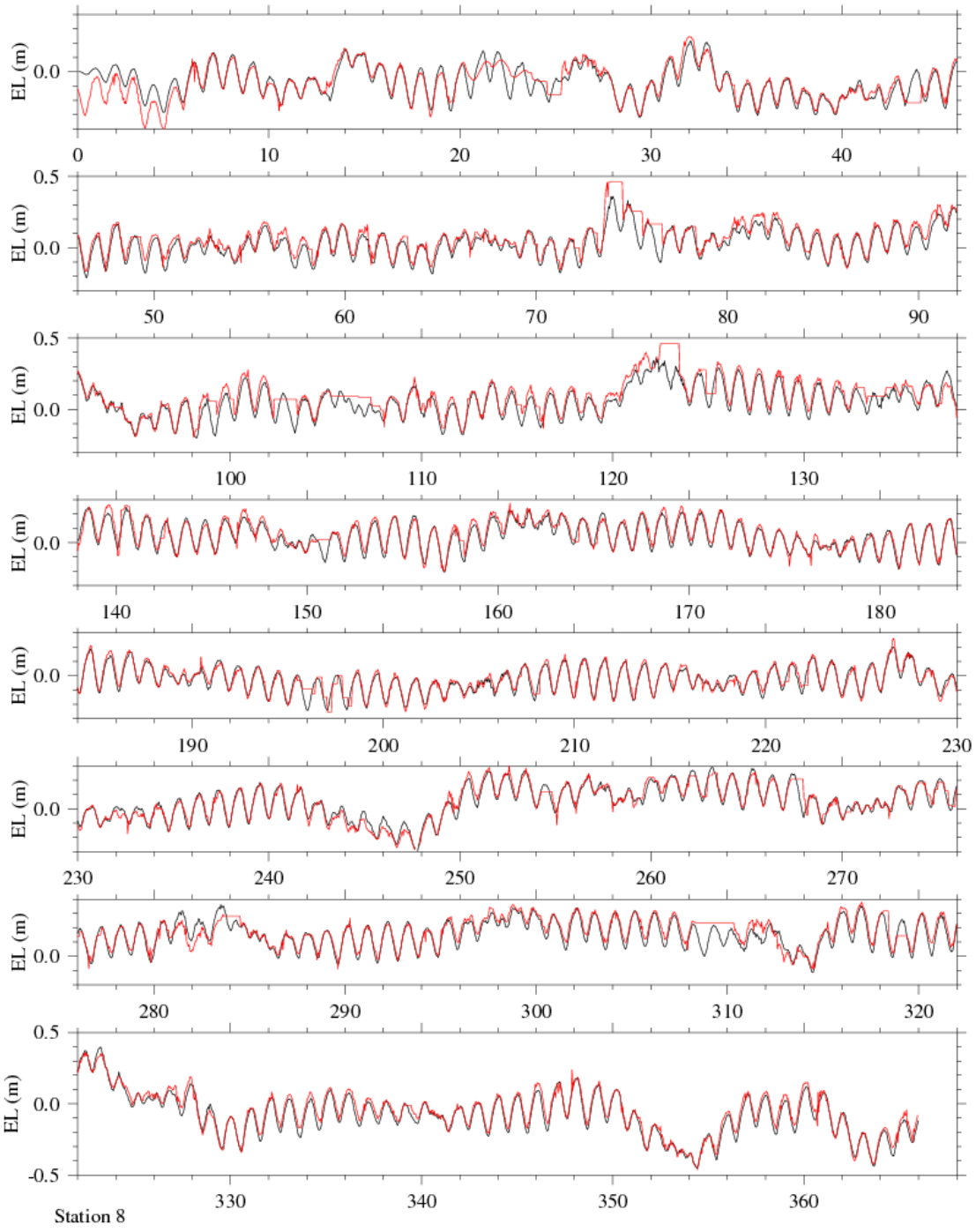

Figure 13. Time series comparison for sea levels observed (red) and modeled (black) at Texas Aquarium.

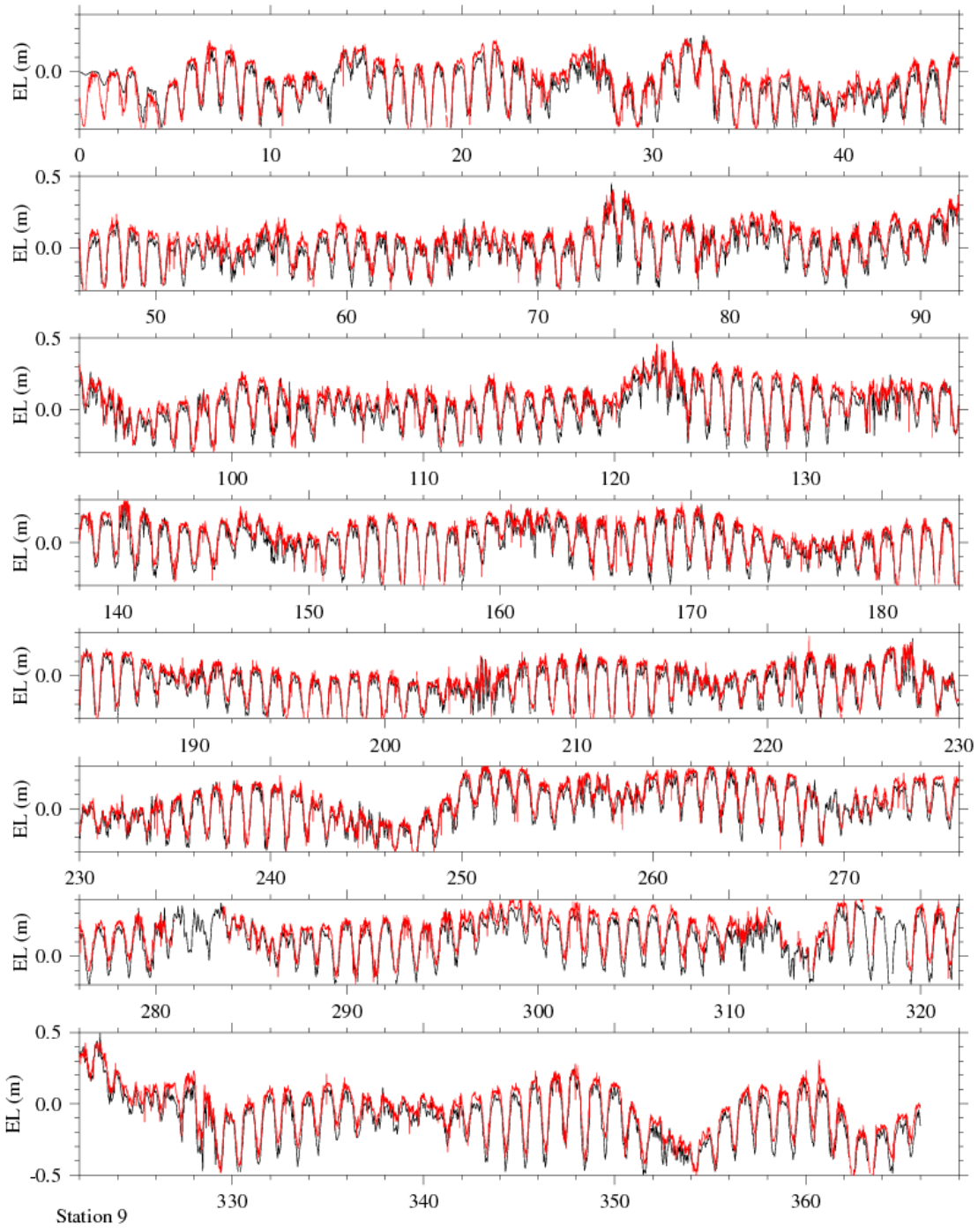

Figure 14. Time series comparison for sea levels observed (red) and modeled (black) at Port Aransas.

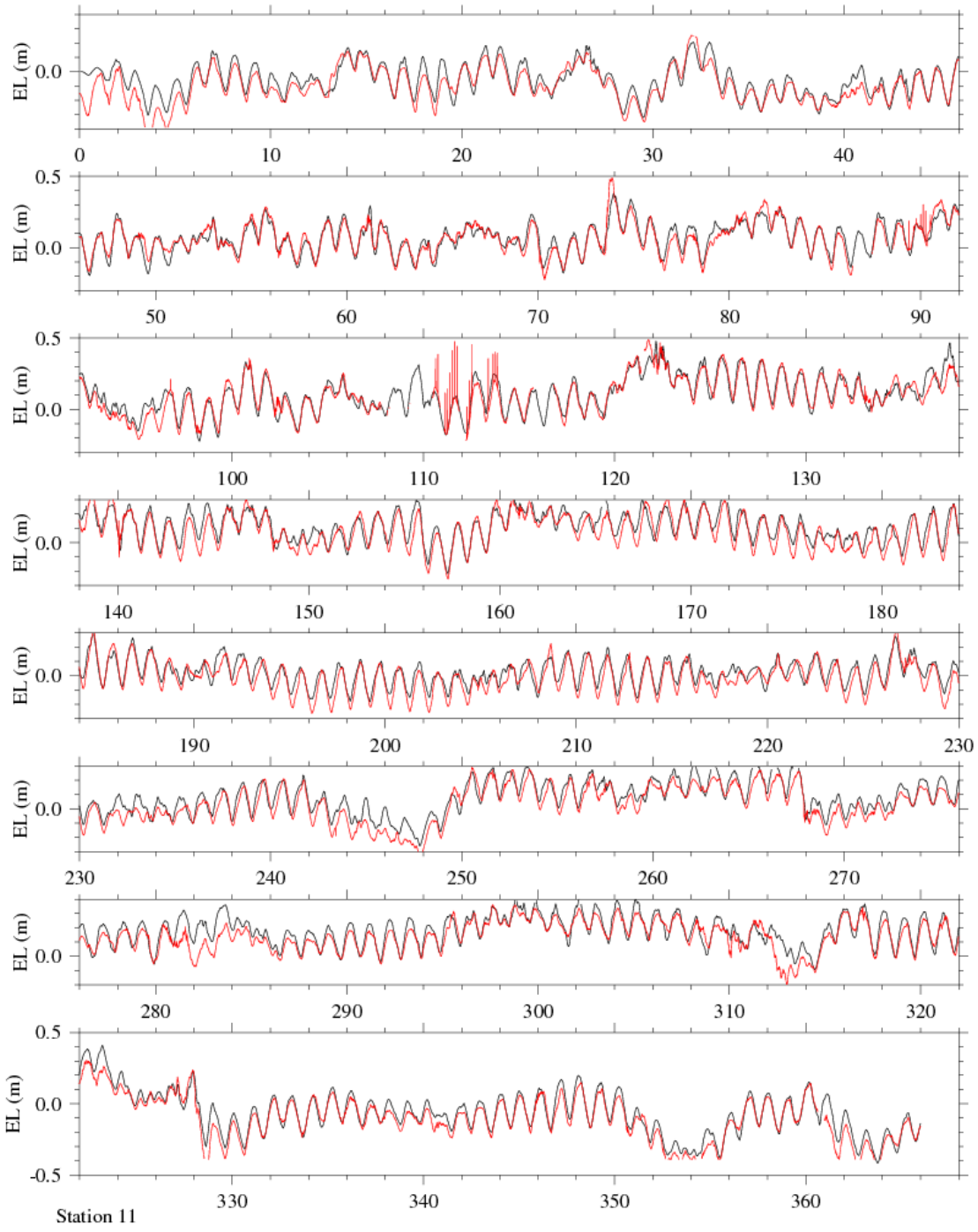

Figure 15. Time series comparison for sea levels observed (red) and modeled (black) at White Point.

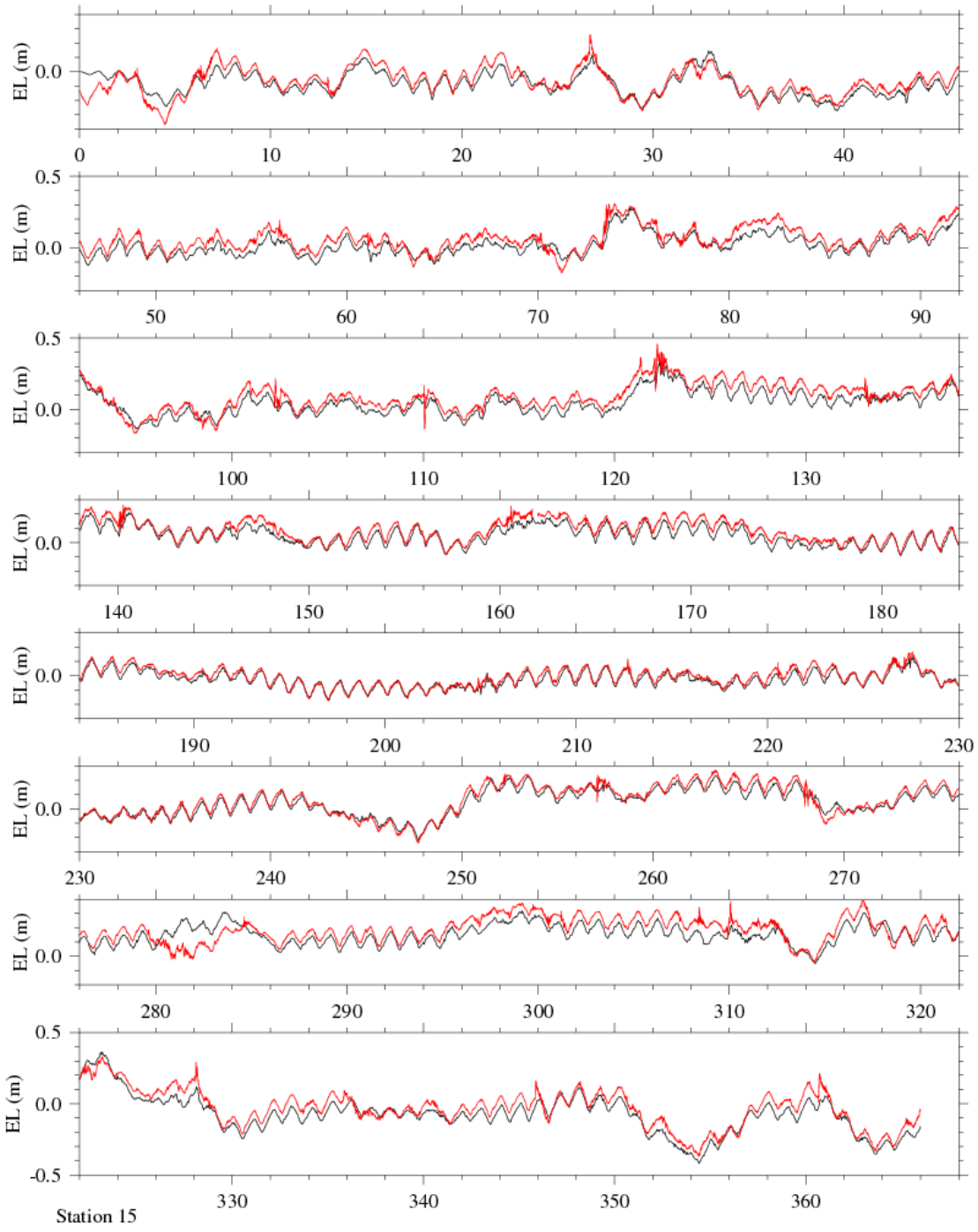

Figure 16. Time series comparison for sea levels observed (red) and modeled (black) at Rockport.

A zoom-in view of the time series comparisons between observed (6-min sampling interval) and modeled (hourly sampling interval) sea levels from day 220 to day 230 in year 2000 is shown in Figure 17.

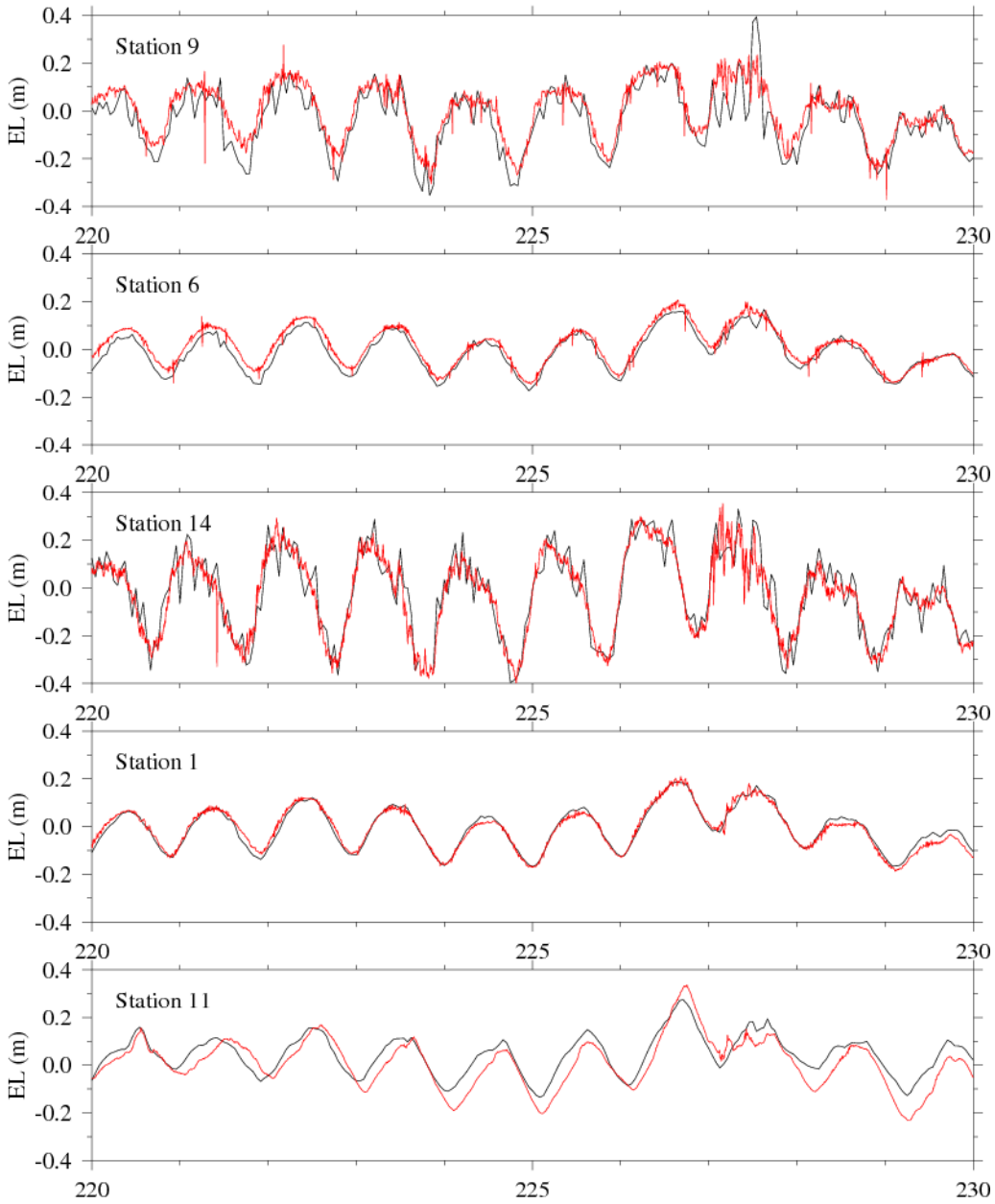

Figure 17. Time series comparison for sea levels observed (red) and modeled (black) at Station 9 (Port Aransas), Station 6 (Ingleside), Station 14 (Bob Hall Pier), Station 1 (Corpus Christi Bay Naval Air Station), and Station 11 (White Point) from day 220 to day 230 in year 2000.

Table 1. Statistical assessment of model performance for 1-year sea level time series

Station	Observation		Model Simulation		Correlation Coefficient	RMSE (m)	Index of Agreement
	Mean (m)	Std. Dev. (m)	Mean (m)	Std. Dev. (m)			
CC Naval Air St	0.03	0.14	0.01	0.13	0.96	0.04	0.98
Packery Channel	0.02	0.11	0.00	0.12	0.96	0.04	0.97
Ingleside	0.05	0.13	0.01	0.13	0.98	0.05	0.97
Texas Aquarium	0.03	0.14	0.02	0.14	0.97	0.03	0.98
Port Aransas	0.03	0.15	-0.02	0.16	0.96	0.07	0.95
White Point	0.03	0.14	0.06	0.14	0.94	0.06	0.96
Rockport	0.05	0.12	0.02	0.11	0.95	0.05	0.96
Bob Hall Pier	-0.01	0.20	-0.01	0.21	0.97	0.05	0.96
Mean					0.96	0.05	0.97

Table 2. Statistical assessment of model performance for 33-hour low-pass filtered sea level time series

Station	Observation		Model Simulation		Correlation Coefficient	RMSE (m)	Index of Agreement
	Mean (m)	Std. Dev. (m)	Mean (m)	Std. Dev. (m)			
CC Naval Air St	0.03	0.12	0.01	0.11	0.97	0.04	0.97
Packery Channel	0.02	0.11	0.00	0.11	0.97	0.03	0.97
Ingleside	0.05	0.11	0.01	0.11	0.98	0.04	0.96
Texas Aquarium	0.04	0.12	0.02	0.11	0.97	0.03	0.98
Port Aransas	0.03	0.11	-0.02	0.11	0.98	0.06	0.94
White Point	0.03	0.13	0.06	0.12	0.96	0.05	0.96
Rockport	0.05	0.11	0.02	0.11	0.96	0.05	0.96
Bob Hall Pier	-0.01	0.12	-0.01	0.12	1.00	0.01	1.00
Mean					0.97	0.04	0.97

Table 3. Comparison of O_1, K_1, and M_2 tidal Harmonic constants. A represents amplitude and θ is phase. Phase angles (in degree) are referred to Greenwich mean time (GMT).

Station	O_1				K_1				M_2			
	Observed		Modeled		Observed		Modeled		Observed		Modeled	
	A (cm)	θ (˚G)	A (cm)	θ (˚G)	A (cm)	θ (˚G)	A (cm)	θ (˚G)	A (cm)	θ (˚G)	A (cm)	θ (˚G)
CC Naval Air St	6.51	95.53	7.13	95.09	6.20	107.80	6.77	108.40	1.62	20.08	1.57	18.54
Packery Channel	3.54	124.10	4.71	107.85	3.29	135.50	4.46	118.95	0.66	67.72	0.91	36.83
Ingleside	6.36	88.17	6.87	85.82	5.88	97.81	6.40	97.07	1.35	352.47	1.29	344.12
Texas Aquarium	6.39	97.57	7.23	94.94	6.24	111.73	6.74	107.78	1.68	17.83	1.63	19.02
Port Aransas	9.63	31.79	10.72	30.42	9.50	39.32	10.35	39.15	5.12	256.83	5.82	256.56
White Point	5.98	118.79	7.30	109.02	6.22	143.52	6.67	125.33	1.33	74.07	1.76	62.30
Rockport	2.98	100.69	2.97	109.56	2.81	105.53	2.88	118.43	0.76	331.48	0.60	333.96
Bob Hall Pier	15.26	17.37	15.26	17.43	15.06	24.87	14.80	26.35	7.89	260.16	7.93	261.57

Quantitative comparisons based on regression analyses and index of agreement (Willmott, 1981; Warner et al, 2005) are given in Table 1. Index of agreement (d) is a model skill first presented by Wilmott (1981) and is defined as

$$d = 1 - \frac{\sum_{i=1}^{N}(P_i - O_i)^2}{\sum_{i=1}^{N}(|P_i - \overline{O}| + |O_i - \overline{O}|)^2}$$

where P and O are modeled (predicted) and observed variables, $\overline{O}$ is time mean of O, and N is the size of the data set. Perfect agreement between model results and observations yields a skill of one and complete disagreement gives a skill of zero.

As can be seen from Table 1, the sea level simulation skill is very high for all stations. The lowest correlation coefficient is 0.94 and the lowest index of agreement is 0.95. The maximum *rms* error is 7 cm, which is about 7% of the sea level variation range. This gives us confidence that our model is capable of simulating the water level variation in high accuracy.

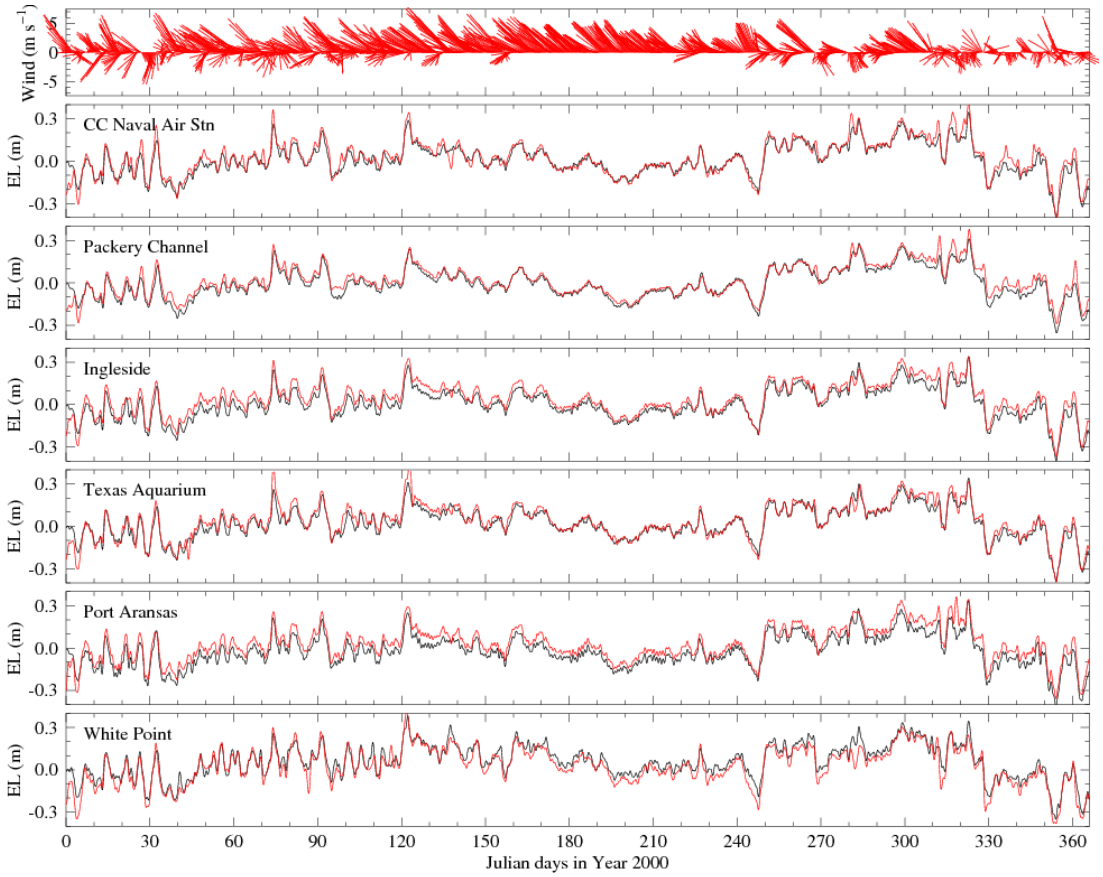

Figure 18. Time series comparison for 33-hour low-pass filtered sea levels observed (red) and modeled (black) at Corpus Christi Bay Naval Air Station, Packery Channel, Ingleside, Texas Aquarium, Port Aransas, and White Point stations, along with the low-passed filtered wind vectors.

Similar visual and quantitative comparisons are shown in Figure 18 and Table 2, respectively, for low pass filtered times series (using a 33-hr half-amplitude filter to distinguish the weather from the tide-induced sea level variations). Included in Figure 18 also are the low-pass filtered wind velocity vectors. The sub-tidal sea level variations are similar at all stations and visual correlations with the wind velocity vectors are clear for many events. For example, for the periods Julian day 31-32, 72-74, 120-122, 248-252, 280-283, and 320-324, the winds are downwelling favorable and sea level has large increases up to about 40 cm, whereas for the periods Julian day 90-93, 122-130, 240-246, and 350-355, the winds are upwelling favorable and sea level decreases by about the same amount. Overall, the means of the correlation coefficients (0.97), indexes of agreement (0.97), and the *rms* errors (4 cm) for the 33-hr low-pass filtered observed and modeled sea level time series are almost the same as the un-filtered time series (Table 1). This gives us confidence in the model accuracy in weather-induced, sub-tidal sea level oscillations. One thing that needs to be pointed out in Figure 18 is that the discrepancy between observed and modeled sea level is larger along the eastern side of Corpus Christi Bay (stations Port Aransas and Ingleside) than the western side (Corpus Christi Bay Naval Air Station, Texas Aquarium and Packery Channel). This may be caused by the fact that the elevation data used for open boundary condition is from Bob Hall Pier which is more close to western Corpus Christi Bay through Packery Channel than to eastern bay through the wider inlet near Port Aransas. Therefore, the uniformity assumption used in specifying elevation open boundary condition (section 3.1) may not be the perfect choice. But the error is relatively small.

To further quantify the tidal simulation veracity we compare harmonic analyses for the principal diurnal tide constituents, O_1 and K_1, and semi-diurnal constituent, M_2 (Table 3). The agreements between observed and modeled amplitudes at the eight stations considered are good. For all three constituents the amplitudes are generally within 1 cm, with the outlier being 1.3 cm. However, since the tidal amplitude is small comparing to wind-driven sub-tidal oscillations inside the Corpus Christi Bay, the errors on phase are relatively large. For example, for O_1 diurnal tide the phases errors are generally within 0.5 - 9˚(2 - 36 min), with the outlier being 16.3˚(65 min). For M2 the phases errors are generally within 0.2 - 8˚(0.4 - 16 min), with the outlier being 31˚(62 min). Both outliers occur at Packery Channel station, which may be related to the relatively coarse horizontal resolution used in that area as well.

4.2 Current velocity

The six ADCP stations relevant to our study are all located in the deep shipping channel (Figure 9, stations 1A, 1B, 2A, 2B, 2C, and 3A). Other ADCP stations are either not functioning or the time series being too short to be useful. The ADCP data are grouped into 5 bins with the center of the bin located at 10%, 30%, 50%, 70%, and 90% of the total depth below the sea surface, respectively. Keep in mind that the near-surface (10% of total depth) and near-bottom (90% of total depth) bins may be contaminated when comparing observed and modeled velocities.

The observed and modeled U and V velocity components from May 5 to May 7, 2000 are shown in Figure 19 – 24, respectively, for the six stations at three observational depths: near-surface (10% depth bin), mid-depth (50% depth bin), and near-bottom (90% depth bin). Since the model employs 31 σ-levels in the vertical we sample it at the σ-layer most closely matching the data sample depth. For stations 1A, 1B, 2A and 2B, as with sea level the visual comparison for the velocity component times series are very good. Both the observations and model show that the current amplitudes decrease with depth. For example, in the Aransas Pass (Stations 1A and 1B) the current amplitudes reach more than 150 cm s^{-1} near the surface and about 100 cm s^{-1} near the bottom. In addition, the diurnal tidal cycle is very clear in the time series and it looks like ebb current is larger than flood current. Since numerical model output is hourly and ADCP observations were not measured at integer hours, vector correlation coefficients, vector orientation differences, and vector regression coefficients between the modeled and observed currents at these stations cannot be calculated.

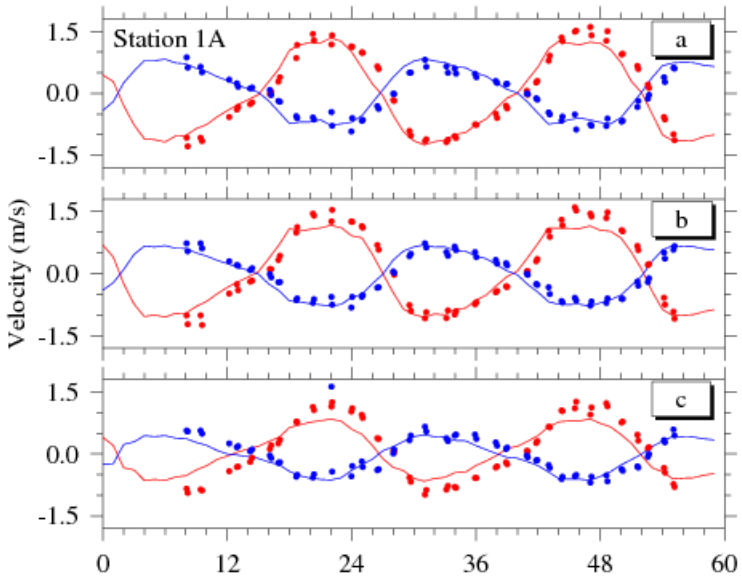

Figure 19. Time series comparison for the U (red) and V (blue) velocity components observed (dot) and modeled (line) at station 1A at three depths: near-surface (a), mid-depth (b) and near-bottom (c)

Station 2C is not located at the main shipping channel of the Corpus Christi Bay. It is actually located at a branch channel which is between Ingleside and Cooks Island. The numerical model horizontal resolution in this area is very coarse. There are only two triangle nodes for the channel cross-section. Therefore, the currents modeled by FVCOM are smaller (on the order of 10 cm s^{-1}) comparing to ADCP observation. In addition, as mentioned above the ADCP measurements may be contaminated since they don't show a clear pattern as illustrated for Station 1A, 1B, 2A, and 2B. This is especially true for the near-surface layer (Figure 23a) and near-bottom layer (Figure 23c).

The simulation result for Station 3A is also not satisfactory. For example, ADCP observation shows that the current is mostly along the shipping channel (V velocity component close to zero due to the orientation of the channel) and at the surface (Figure 24a) U velocity is eastward, in the middle almost zero (Figure 24b), and near the bottom it is westward (Fig 24c). The bottom current speed is larger than that of surface current.

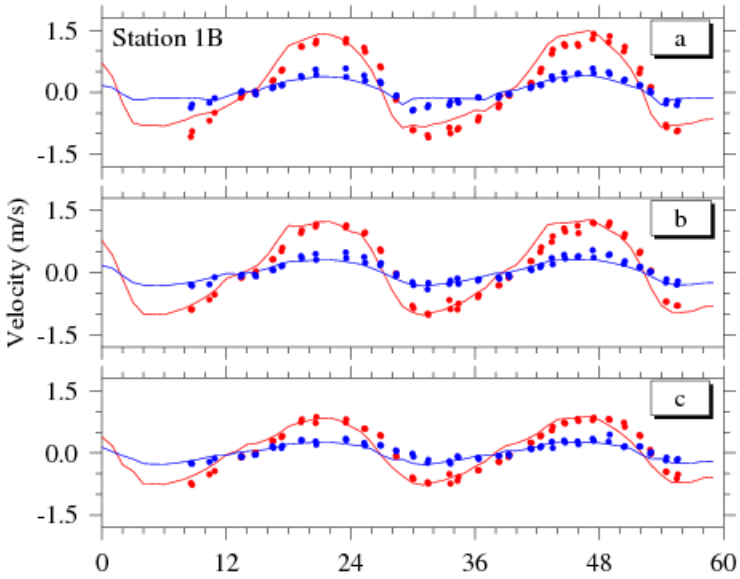

Figure 20. Time series comparison for the U (red) and V (blue) velocity components observed (dot) and modeled (line) at station 1B at three depths: near-surface (a), mid-depth (b) and near-bottom (c)

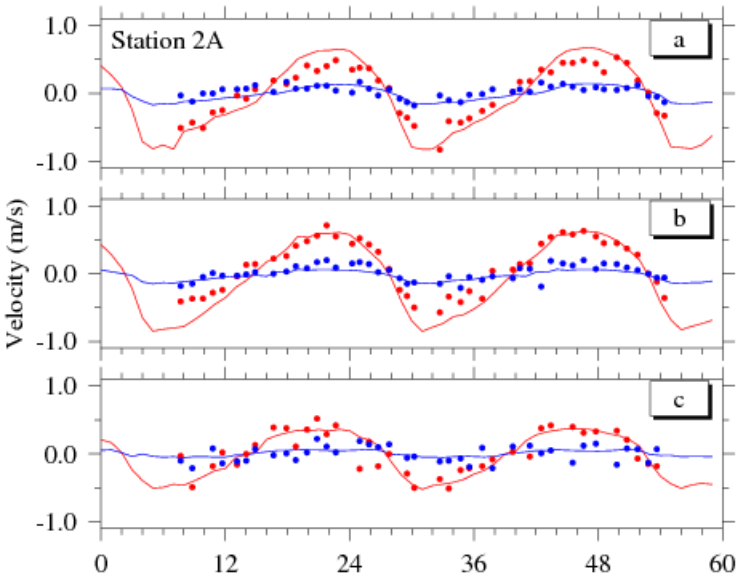

Figure 21. Time series comparison for the U (red) and V (blue) velocity components observed (dot) and modeled (line) at station 2A at three depths: near-surface (a), mid-depth (b) and near-bottom (c)

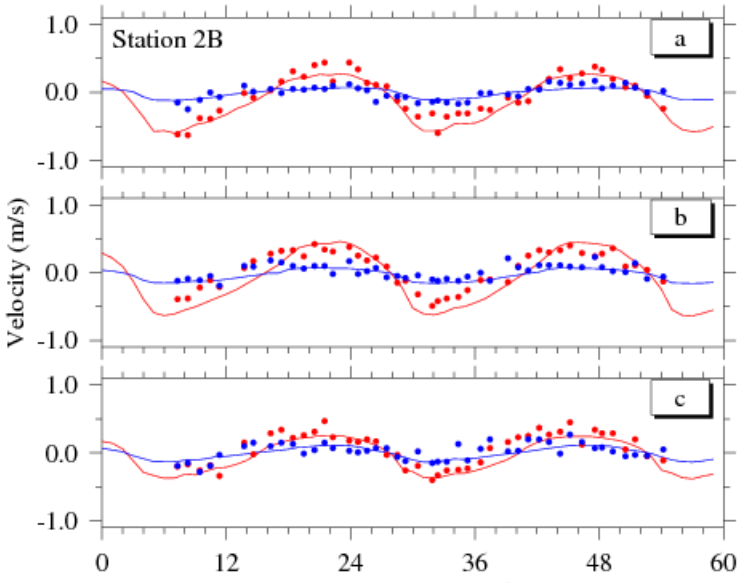

Figure 22. Time series comparison for the U (red) and V (blue) velocity components observed (dot) and modeled (line) at station 2B at three depths: near-surface (a), mid-depth (b) and near-bottom (c)

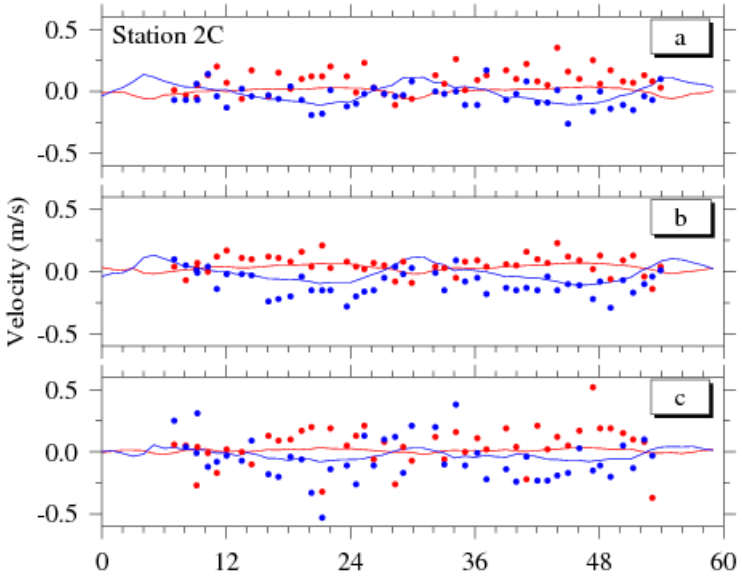

Figure 23. Time series comparison for the U (red) and V (blue) velocity components observed (dot) and modeled (line) at station 2C at three depths: near-surface (a), mid-depth (b) and near-bottom (c)

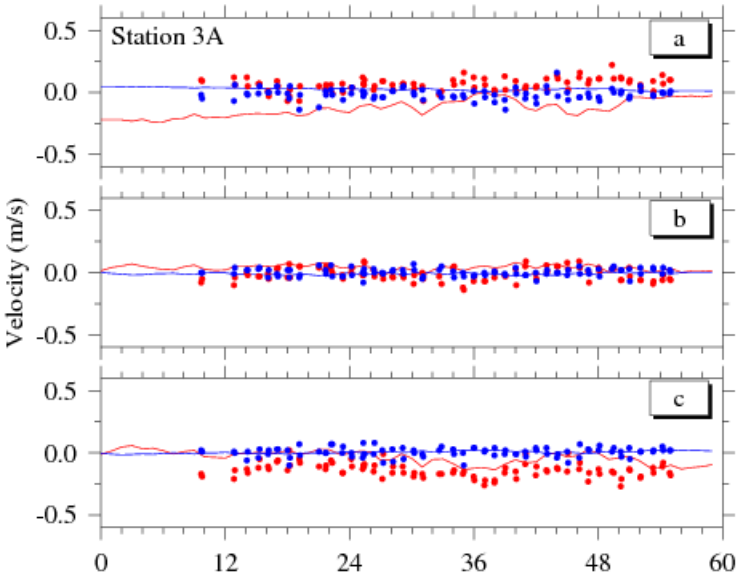

Figure 24. Time series comparison for the U (red) and V (blue) velocity components observed (dot) and modeled (line) at station 3A at three depths: near-surface (a), mid-depth (b) and near-bottom (c)

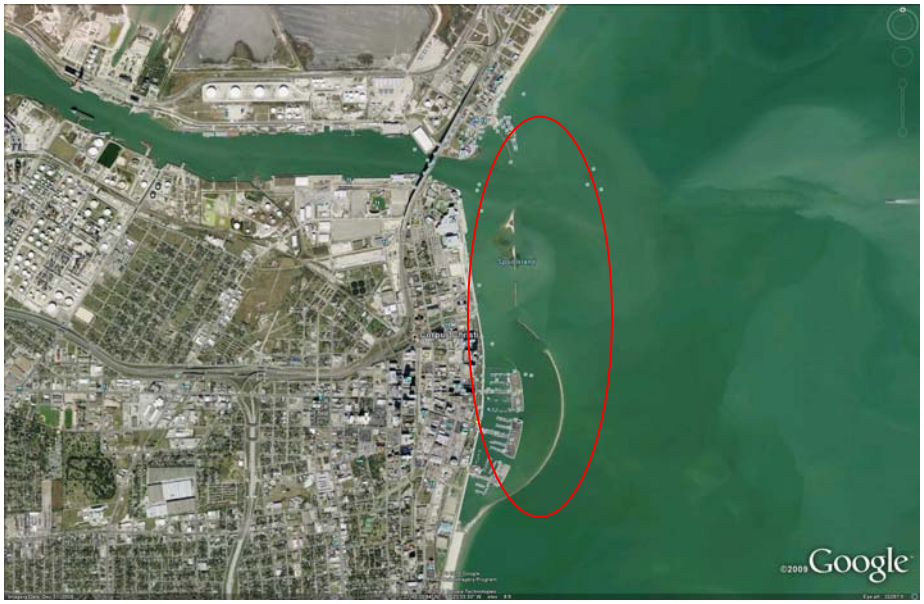

Figure 25. Google image of the harbor entrance in Corpus Christi Bay. The spoil islands and other constructions (see the red oval) are not included in the Corpus Christi Bay model grid

On the contrary, in our model result westward currents are mostly concentrated in the surface during this period of time and they are relatively small at mid-depth and near bottom. Possible reasons for this discrepancy may exist in: 1) coarse numerical model horizontal resolution near the harbor bridge; 2) some small scale structures not included

in the numerical model and maybe causing small scale current pattern, such as bridge pier, moving ships; 3) the most important error may come from not including in the numerical model mesh all the spoil islands near the harbor entrance (see Figure 25).

The vertical profiles of observed and modeled U and V velocity components are shown in Figures 26 – 31. Since ADCP measurements weren't taken at integer hour number, linear interpolation is used to estimate the observed velocity profiles at integer hours. Keep in mind that this may cause errors. The conclusion drawn from the comparison in Figure 26 – 31 is similar to that from horizontal current comparison in Figure 19 – 24. For Stations 1A, 1B, 2A, and 2B, the results are reasonably good, while for stations 2C and 3A it may indicate that the model is incapable of yielding accuracy simulation at certain locations due to coarse horizontal resolution and other model drawbacks.

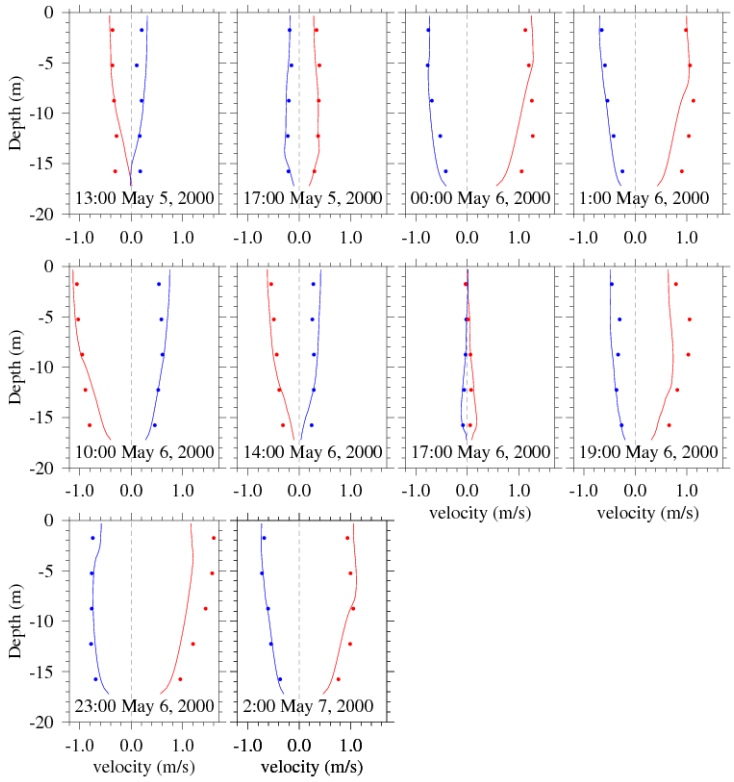

Figure 26. Vertical profile of U (red) and V (blue) velocity components observed (dot) and modeled (line) at station 1A at various times.

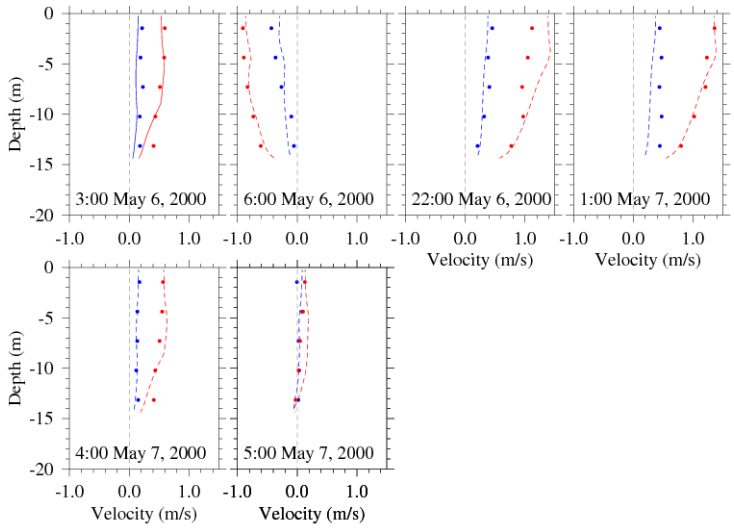

Figure 27. Vertical profile of U (red) and V (blue) velocity components observed (dot) and modeled (line) at station 1B at various times.

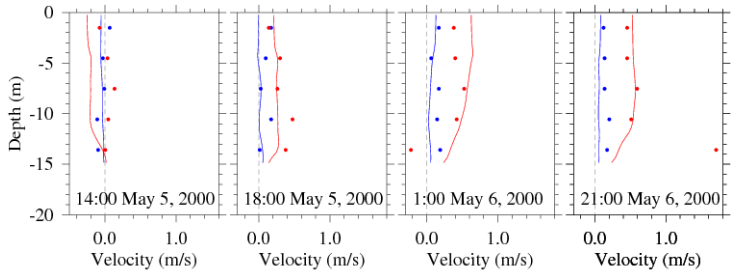

Figure 28. Vertical profile of U (red) and V (blue) velocity components observed (dot) and modeled (line) at station 2A at various times.

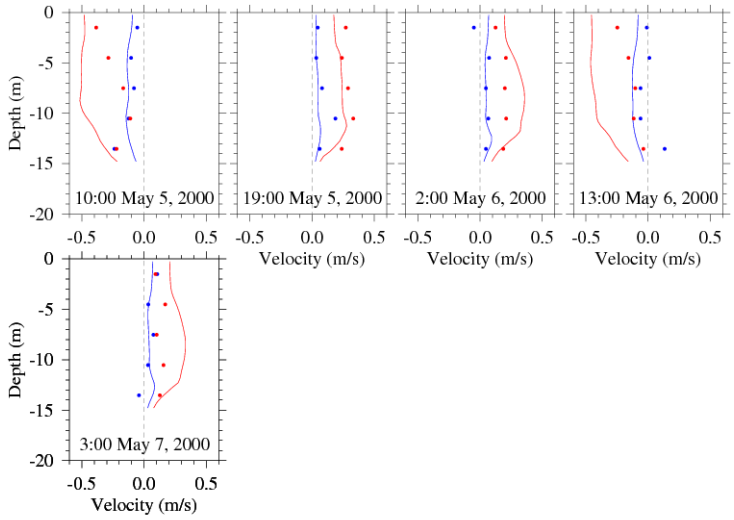

Figure 29. Vertical profile of U (red) and V (blue) velocity components observed (dot) and modeled (line) at station 2B at various times.

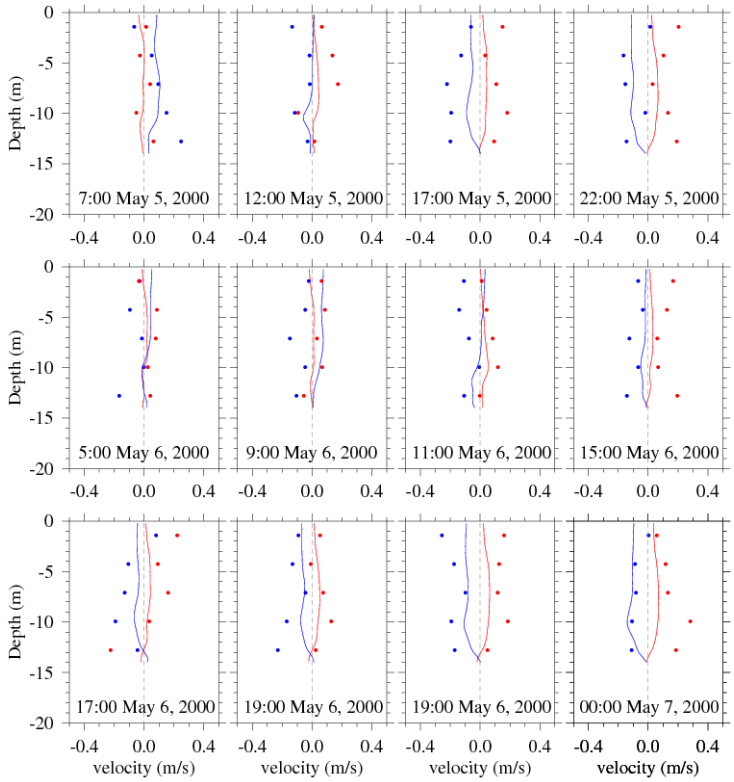

Figure 30. Vertical profile of U (red) and V (blue) velocity components observed (dot) and modeled (line) at station 2C at various times.

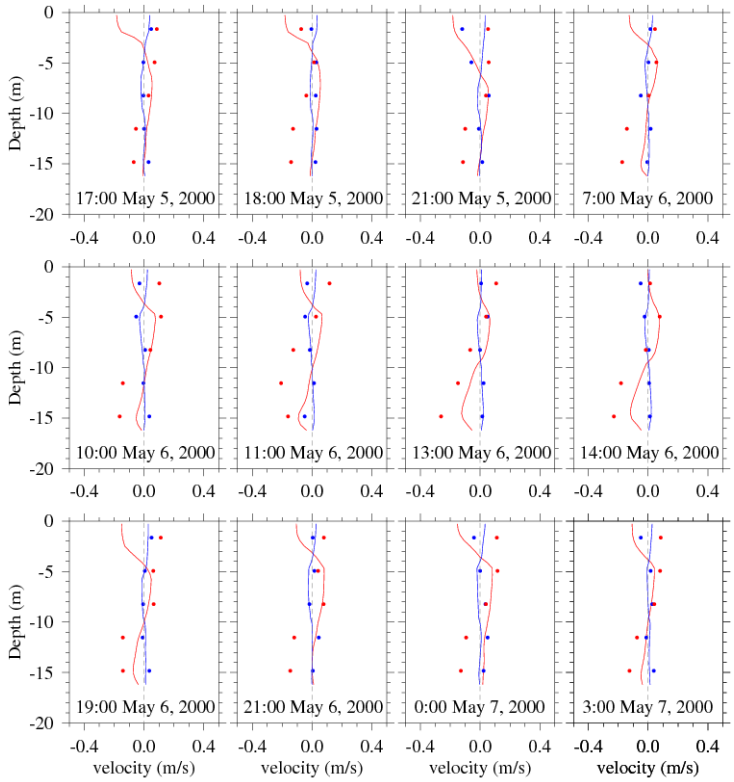

Figure 31. Vertical profile of U (red) and V (blue) velocity components observed (dot) and modeled (line) at station 3A at various times.

4.3 Salinity

There are two sets of salinity data. The first one was measured during the same time period as the ADCP observation (May 5 – May 7, 2000). Three stations were available (Figure 9, Stations 1B, 2A, and 3A). Salinity data was measured manually with a CTD probe in the center of the transect during both descent and ascent. Only measurements at integer hour are used, since numerical model output is hourly. We choose salinity at a node point that is closest to the observational site to represent the modeled salinity values. No interpolation is used. The comparisons between observed and modeled vertical salinity profiles are shown in Figures 32 – 34. As can be seen, the maximum difference for salinity simulation is about 1.5 ppt for Stations 1B and 2A and about 4.0 ppt for Station 3A. In addition, the observed salinity profiles at Stations 1B and 2A are mostly vertically uniform while the modeled salinity profiles have a weak stratification with bottom salinity greater than surface salinity by about 0.5 – 1 ppt. This error is probably caused by the weaker vertical turbulent mixing coefficient predicted by Mellor-Yamada turbulence closure model embedded in FVCOM. For Station 3A the discrepancy is more obvious. Modeled salinity is consistently smaller than the observed ones by 2.5 - 4.0 ppt. I believe this may be attributed to inaccurate inflow data at the Nueces River (see more explanation below).

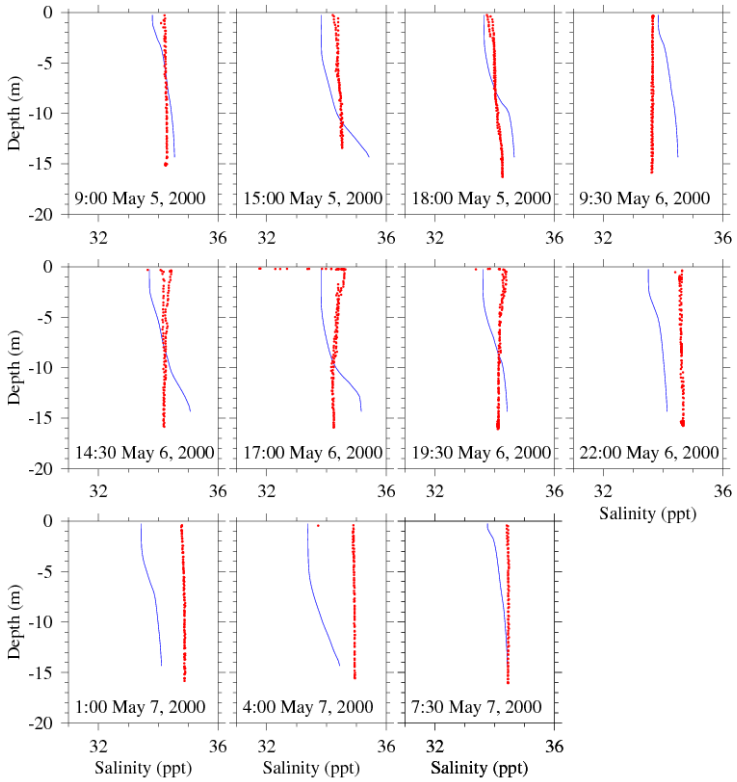

Figure 32. Vertical profile of salinity observed (red dot) and modeled (blue line) at station 1B at various times.

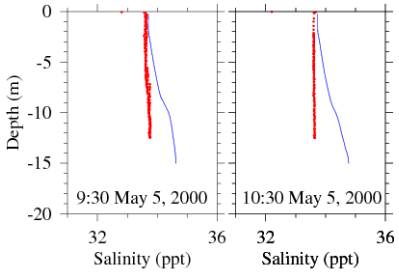

Figure 33. Vertical profile of salinity observed (red dot) and modeled (blue line) at station 2A at various times.

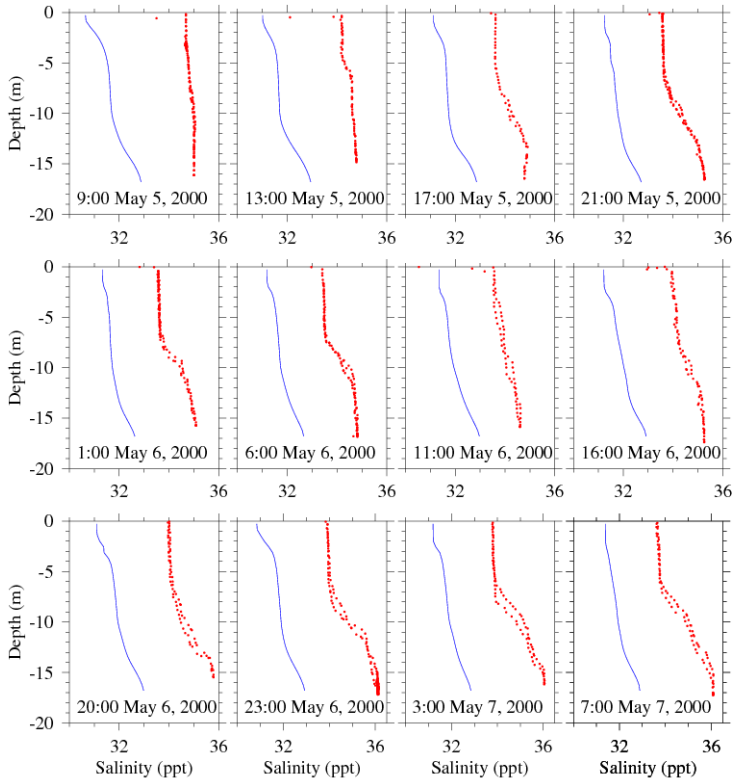

Figure 34. Vertical profile of salinity observed (red dot) and modeled (blue line) at station 3A at various times.

The other type of salinity data is long-term salinity observations in the Nueces Bay, the Corpus Christi Bay, the Aransas Bay, and the upper Laguna Madre at intersection of JFK causeway and GIWW. However, the accuracy of measurements is questionable as will be illustrated in the following figures. Additionally, the depth at which salinity values were measured is unknown. Hence, in the figures shown below we choose model result at mid-depth (sigma layer 15) to compare with observation. Figures 35 – 40 show the time series of observed and modeled salinity at various locations. For the three TWDB stations (Figure 35 - 37), the abrupt jump in measured salinity values make me wonder the quality of the observations. In addition, in Corpus Christi Bay the salinity between TWDB observation and Paul Montagna's data can be as large as 12 ppt for certain periods of time. Since the two locations are relatively close, if both data are accurate then it indicates that there exists a strong salinity front in the bay which is not very likely. If we assume the measurements are correct, then the modeled salinities have errors as large as 5 ppt at the Corpus Christi Bay station, 18 ppt at the Aransas Bay station, and 13 ppt at the upper Laguna Madre station. For the salinity simulation in the Nueces Bay, the accuracy in specifying Nueces River inflow has an important influence. The calculation results (Figures 38 and 39) show that normally the calculated salinity is smaller than the observed one. This may be caused by two reasons, either the inflow condition is inaccurate or some important processes are missing in the numerical model. One plausible reason is that the Nueces Delta is omitted in the numerical model. If you

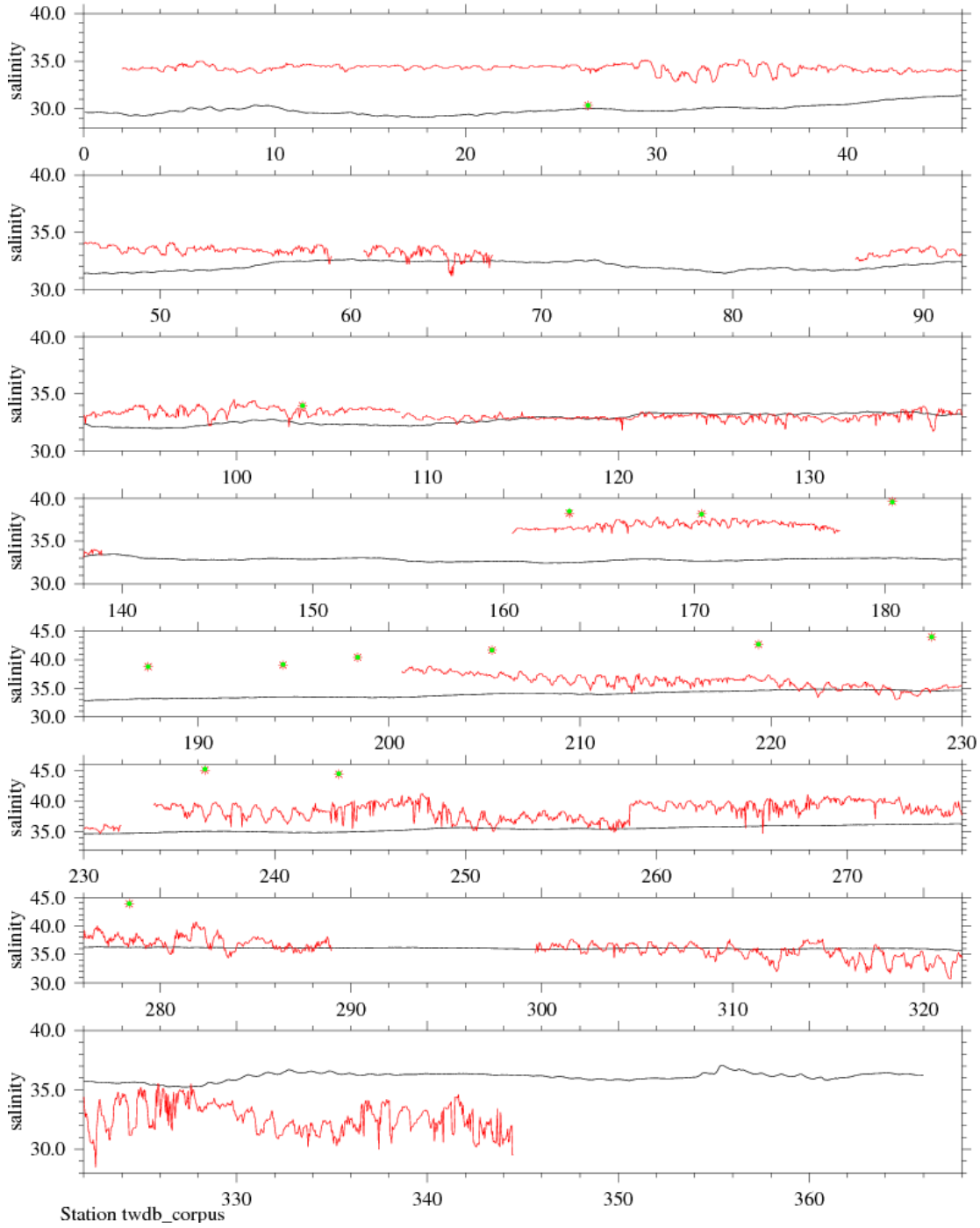

Figure 35. Time series comparison for salinities observed (red) and modeled (black) at TWDB station Corpus Christi Bay near Ingleside at range marker. Green and red dots are from Paul Montagna's hypoxia program measurements (personal communication).

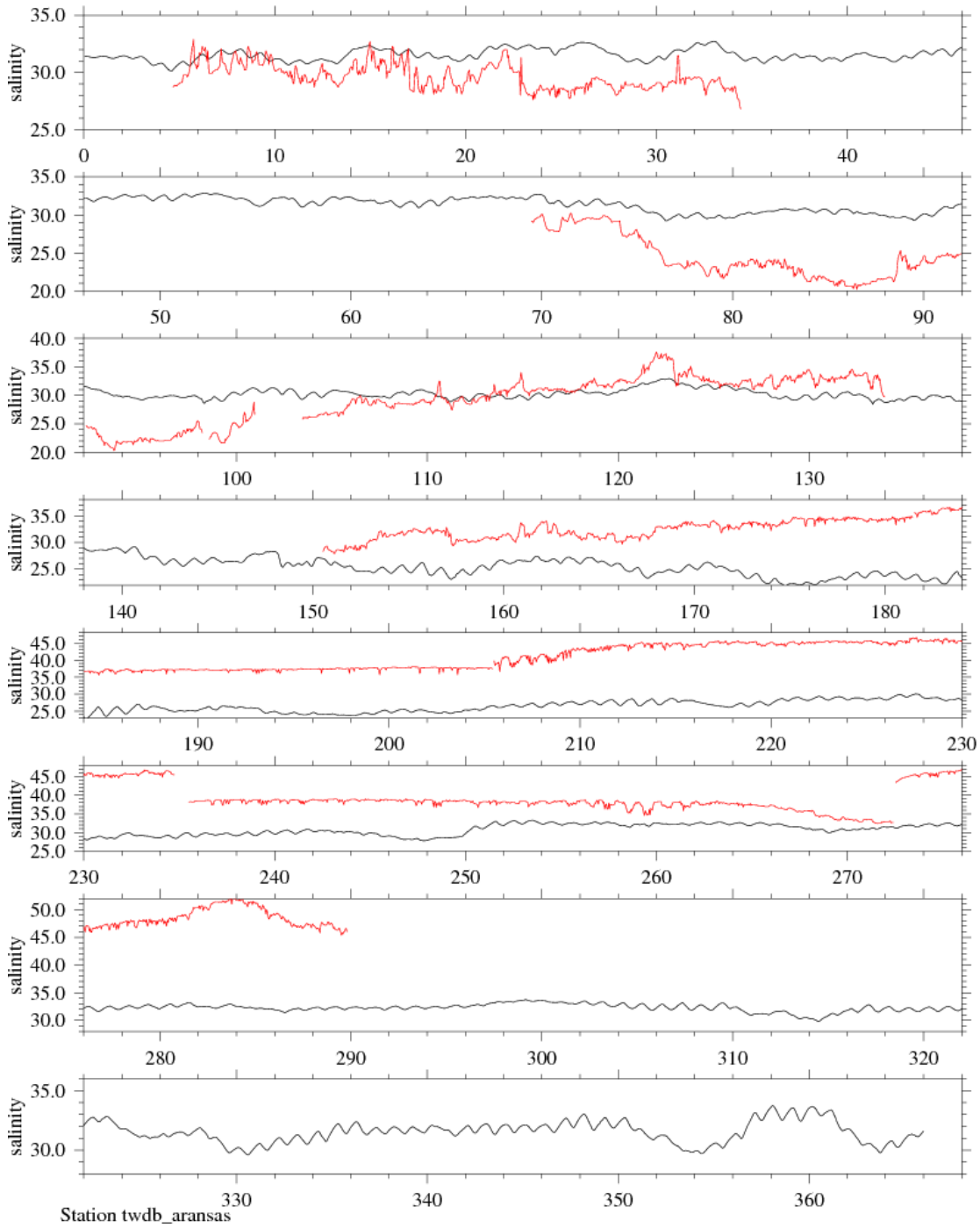

Figure 36. Time series comparison for salinities observed (red) and modeled (black) at TWDB station Aransas Bay east of Rockport.

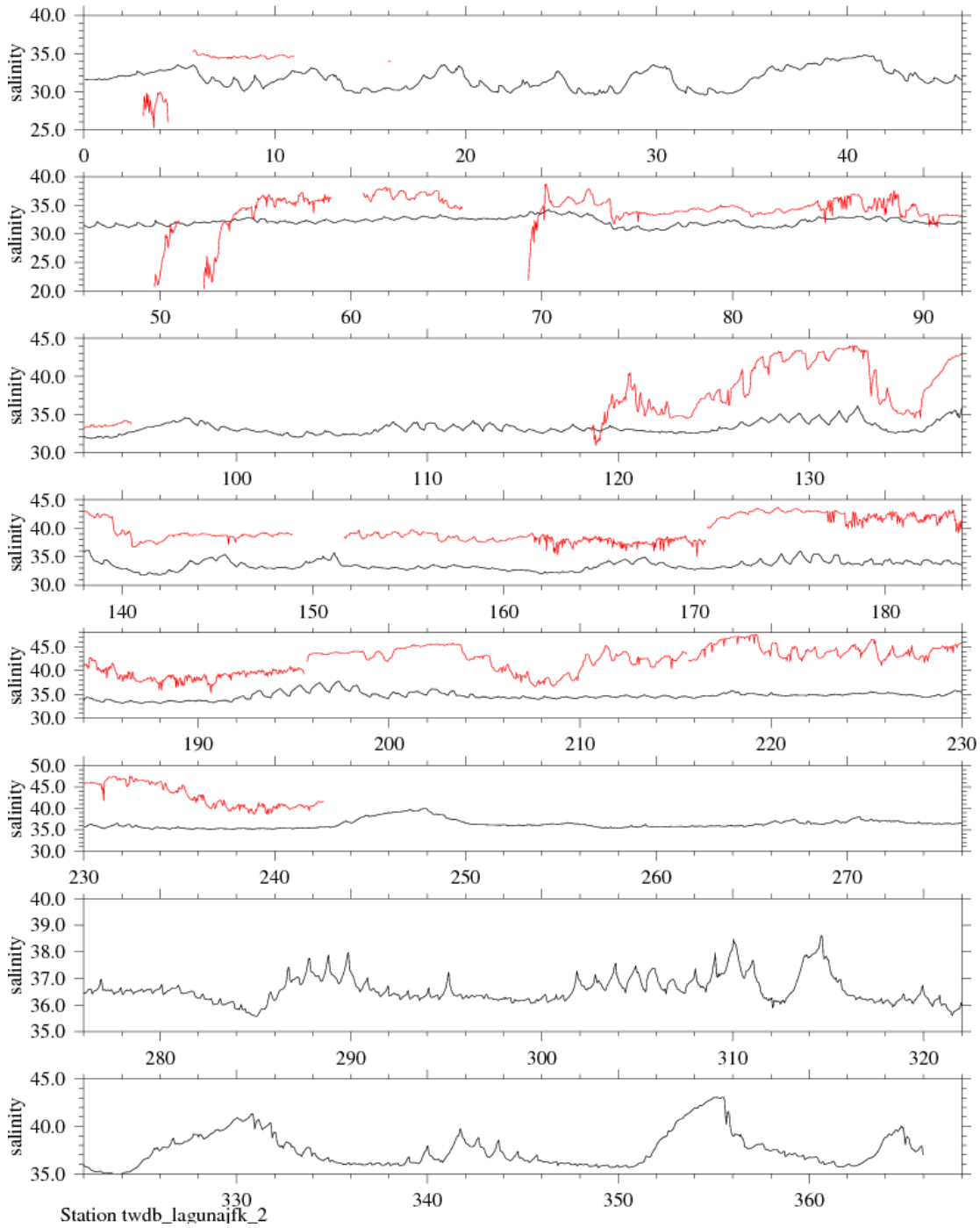

Figure 37. Time series comparison for salinities observed (red) and modeled (black) at TWDB station Laguna Madre at JFK Causeway and ICWW intersection.

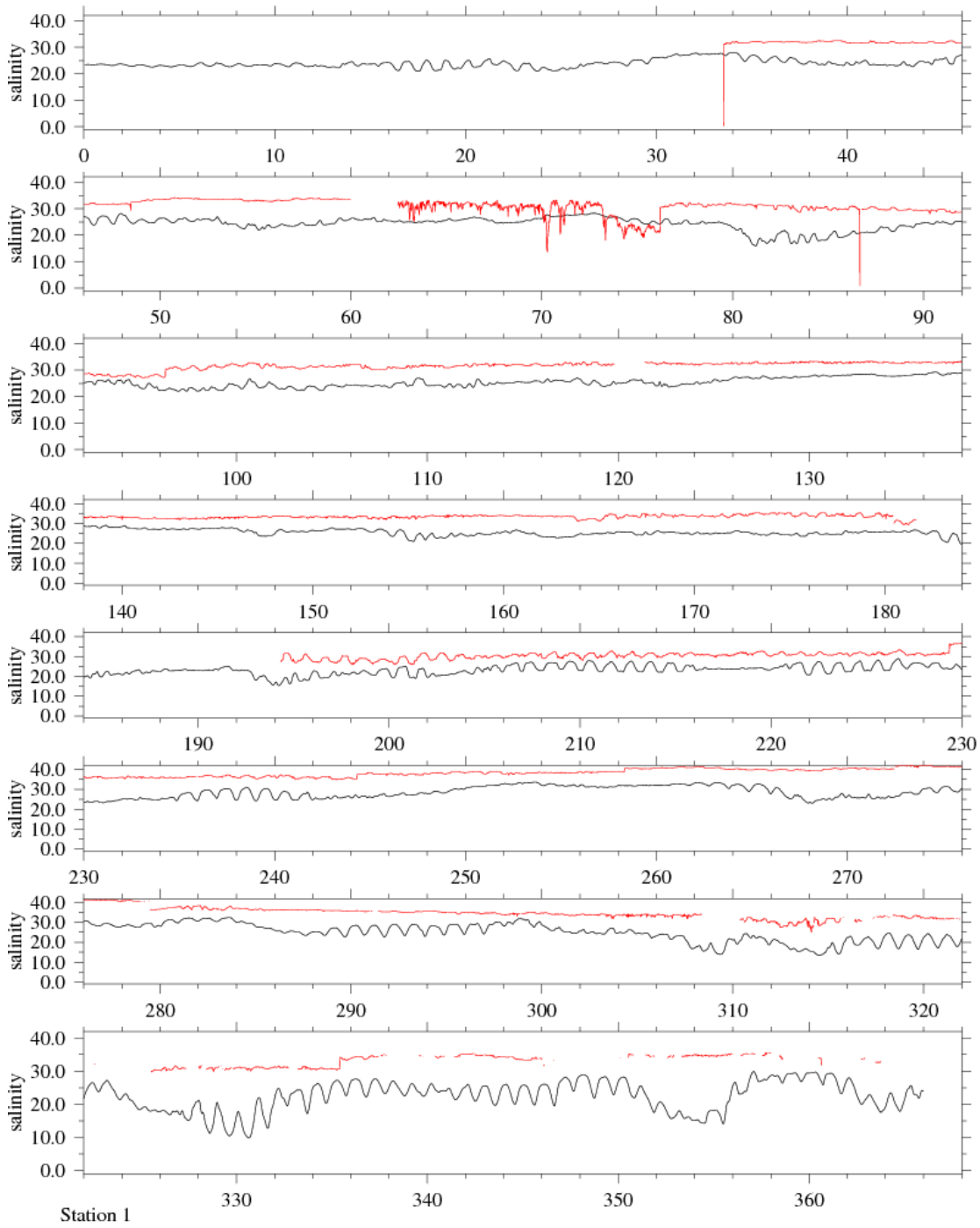

Figure 38. Time series comparison for salinities observed (red) and modeled (black) at TCOON station 01.

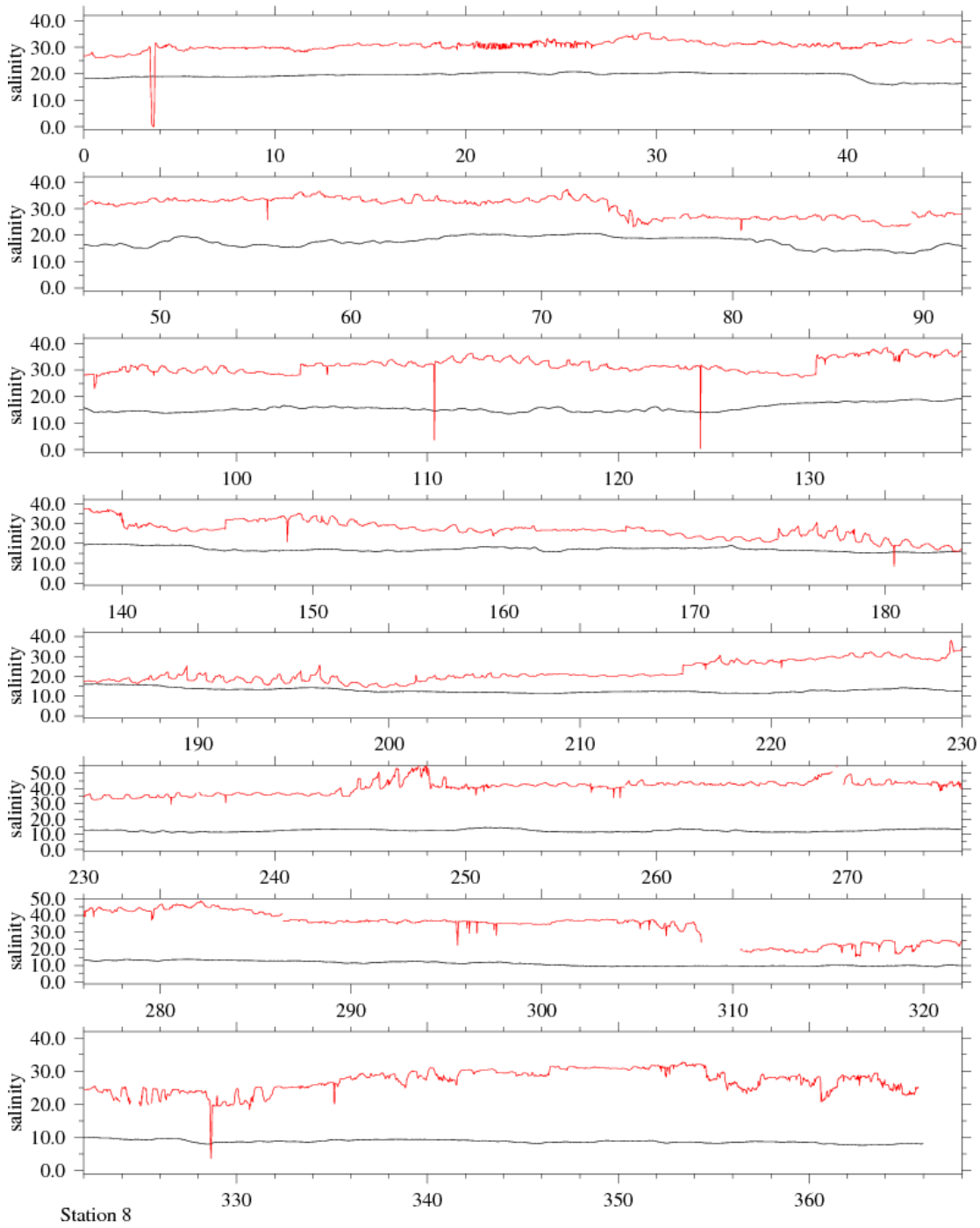

Figure 39. Time series comparison for salinities observed (red) and modeled (black) at TCOON station 08.

look at the TCOON website and compare the real time salinity measurement along the Nueces Delta, you will find that higher salinities (may reach 40 to 50 ppt) are located in the upper stream part. One explanation is that shallow area makes the evaporation effect more dominant. Therefore, the Nueces Delta acts as a high salinity source for this area. This may explain why at station 08, the maximum difference between observed and modeled salinity can be as large as 35 ppt for certain times. Of course, the assumption of evaporation and precipitation being spatially uniform may also worsen the problem.

To summarize possible reasons for salinity simulation discrepancy, I list the following facts: 1) In numerical experiment, the precipitation and evaporation data are from one observation station and uniformly interpolated to all model grid points. In reality this uniform distribution is definitely not the case and errors are brought into the model. 2) Open boundary salinity variation is also from one observation station and it is assumed that salinity of all open boundary nodes follows this same time series. 3) Nueces River Delta is very roughly depicted by the numerical model mesh. This causes error in the salinity calculation for stations in the Nueces Bay (related to reason 5 below) and in the Corpus Christi Bay (since the Nueces Bay is located at the upstream part of the Corpus Christi Bay). 4) The Nueces River inflow data may have error. 5) All intertidal zones (marshes and wetlands) and some very shallow area are not included in the computation domain, where, I believe, are the most plausible places to generate high salinity waters due to high evaporation rate.

5. Conclusion

The Finite-Volume Coastal Ocean Model (FVCOM) has been applied to the Corpus Christi Bay region to simulate the three-dimensional circulation driven by buoyancy, tides, and winds. Comparisons between observations and model simulation show that FVCOM is very accurate in simulating the sea level oscillations. The average correlation coefficient and Index of Agreement are 0.96 and 0.97, respectively, for the total water level elevation, and 0.97 and 0.97, respectively, for the sub-tidal, wind-driven oscillations. The velocity simulation is visually consistent with available ADCP measurements. However, no quantitative assessment can be done due to the short duration and non-uniform interval of observed current time series. The salinity simulation is not as satisfactory as sea level and current velocity. There are several reasons for this discrepancy. The quality of salinity observation may be one problem. The uncertainties in external forcings, such as the assumption that precipitation and evaporation are distributed uniformly in the space, may also make the calculation worse. The omission of shallow areas in order to avoid wetting and drying algorithm may make the water fresher in these regions, which is the case near the Nueces Delta.

To improve simulation accuracy, especially for salinity, I have the following recommendations:

1) Collect meteorological forcing data at several stations near Corpus Christi Bay, so that spatially varying external forcing data can be specified for the model. Another choice is

to use products from a local-scale high-resolution numerical weather prediction model (such as WRF model results).
2) Collect long-term ADCP current measurements at a few stations in the Bay. QA (quality assurance) and QC (quality control) are important.
3) Include the Nueces Delta and other wetlands in the model domain; allow wetting and drying in the numerical calculation.
4) Refine model grid (with the high performance computing power we have nowadays, it is affordable)
5) Couple this model to a gulf scale circulation model so that open boundary conditions are more accurate. Of course, we can also try to set up a model for the whole Texas coastal area.

6. References

Chen, C., H. Liu, and R. C. Beardsley (2003), An unstructured grid, finite-volume, three-dimensional, primitive equations ocean model: Application to coastal ocean and estuaries. *J. Atmos. Oceanic Technol.,* **20**, 159-186.

Chen, C., R. C. Beardsley, and G. Cowles (2006), An unstructured grid, finite-volume coastal ocean model: FVCOM user manual. School for Marine Science and Technology, University of Massachusetts Dartmouth, 315 pp.

Galperin, B., L.H. Kantha, S. Hassid, and A. Rosati (1988), A quasi-equilibrium turbulent energy model for geophysical flows. *J. Atmos. Sci*., **45**, 55-62.

Huang, R.X. (1993), Real freshwater flux as a natural boundary condition for the salinity balance and thermohaline circulation forced by evaporation and precipitation. *J. phys. Oceanogr*., **23**, 2428-2446.

LeVeque, R.J. (2002), *Finite Volume Methods for Hyperbolic Problems*. Cambridge University Press, 558 pp.

Mellor, G.L., and T. Yamada (1982), Development of a turbulence closure model for geophysical fluid problem. *Rev. Geophys. Space. Phys*., **20**, 851-875.

Montagna, P.A., and R.D. Kalke (1995), Ecology of infaunal Mollusca in south Texas estuaries. *Am. Malacol. Bull*., **11**, 163-175.

Smagorinsky, J. (1963), General circulation experiments with the primitive equations, I. The basic experiment. *Mon. Wea. Rev.*, **91**, 99-164.